ANTIOXIDANTS & REDOX SIGNALING
Volume 24, Number 8, 2016
© Mary Ann Liebert, Inc.
DOI: 10.1089/ars.2015.6363

ORIGINAL RESEARCH COMMUNICATION

# Targeted Nitric Oxide Delivery by Supramolecular Nanofibers for the Prevention of Restenosis After Arterial Injury

Edward S.M. Bahnson,[1,2,*] Hussein A. Kassam,[1,2,*] Tyson J. Moyer,[1,3] Wulin Jiang,[1,2] Courtney E. Morgan,[1,2] Janet M. Vercammen,[1,2] Qun Jiang,[1,2] Megan E. Flynn,[1,2] Samuel I. Stupp,[1,3–6,†] and Melina R. Kibbe[1,2,†]

## Abstract

***Aims:*** Cardiovascular interventions continue to fail as a result of arterial restenosis secondary to neointimal hyperplasia. We sought to develop and evaluate a systemically delivered nanostructure targeted to the site of arterial injury to prevent neointimal hyperplasia. Nanostructures were based on self-assembling biodegradable molecules known as peptide amphiphiles. The targeting motif was a collagen-binding peptide, and the therapeutic moiety was added by S-nitrosylation of cysteine residues. ***Results:*** Structure of the nanofibers was characterized by transmission electron microscopy and small-angle X-ray scattering. S-nitrosylation was confirmed by mass spectrometry, and nitric oxide (NO) release was assessed electrochemically and by chemiluminescent detection. The balloon carotid artery injury model was performed on 10-week-old male Sprague-Dawley rats. Immediately after injury, nanofibers were administered systemically *via* tail vein injection. S-nitrosylated (S-nitrosyl [SNO])-targeted nanofibers significantly reduced neointimal hyperplasia 2 weeks and 7 months following balloon angioplasty, with no change in inflammation. ***Innovation:*** This is the first time that an S-nitrosothiol (RSNO)-based therapeutic was shown to have targeted local effects after systemic administration. This approach, combining supramolecular nanostructures with a therapeutic NO-based payload and a targeting moiety, overcomes the limitations of delivering NO to a site of interest, avoiding undesirable systemic side effects. ***Conclusion:*** We successfully synthesized and characterized an RSNO-based therapy that when administered systemically, targets directly to the site of vascular injury. By integrating therapeutic and targeting chemistries, these targeted SNO nanofibers provided durable inhibition of neointimal hyperplasia *in vivo* and show great potential as a platform to treat cardiovascular diseases. *Antioxid. Redox Signal.* 24, 401–418.

## Introduction

Cardiovascular interventions, such as angioplasty, stenting, or bypass grafting, have limited durability due to eventual arterial restenosis and occlusion. This reocclusive process initiated at the site of intervention is complex and multifactorial and involves inflammation, cellular proliferation, and cellular migration, among other events (7–9). Ultimately, this arterial injury response leads to the development of neointimal hyperplasia, which narrows the arterial lumen. Development of a therapy that effectively prevents the formation of neointimal hyperplasia while simultaneously stimulating reendothelialization is a significant unmet clinical need. In this context, nitric oxide (NO) is an ideal therapeutic

[1]Simpson Querrey Institute for BioNanotechnology, Northwestern University, Chicago, Illinois.
[2]Department of Surgery, Feinberg School of Medicine, Northwestern University, Chicago, Illinois.
Departments of [3]Materials Science and Engineering and [4]Chemistry, Northwestern University, Evanston, Illinois.
[5]Department of Medicine, Feinberg School of Medicine, Northwestern University, Chicago, Illinois.
[6]Department of Biomedical Engineering, Northwestern University, Evanston, Illinois.
*These two authors contributed equally and share first authorship.
†These two authors contributed equally and share senior authorship.

**Innovation**

Even though nitric oxide (NO) has great therapeutic potential, NO-based therapies have not been successfully translated to the clinical arena due to many practical challenges. Among those challenges is the need for a specific local effect, while avoiding undesirable systemic effects. To our knowledge, this is the first report of a systemically delivered NO-based therapy that directs the biological effect of NO to the site of interest, thereby avoiding systemic side effects. Even though our work only addresses treatment to the injured vasculature, this work has far-reaching implications for other disease processes that may benefit from targeted systemic delivery of therapeutic agents.

agent due to its many vasoprotective properties (17, 18, 28, 45), including inhibition of the processes that lead to neointimal hyperplasia (11, 16, 19, 29, 30, 34, 40, 42, 46, 47, 57, 59).

Furthermore, NO is known to promote the reformation of an intact endothelial layer following injury (60). However, NO is a challenging molecule to deliver owing to its short half-life, rapid metabolism, and reactivity (27). Chemically stable and biocompatible nanostructures with targeting capacity and the ability to deliver NO *in vivo* could overcome many of these challenges. Nanostructures are advantageous as they can display small molecules (25), aptamers (14), antibodies (44), and proteins (6, 12) on their surfaces to release therapeutics at a targeted site (56). Most work in this area has focused on cancer therapies, with very few examples targeting cardiovascular pathologies (5). Examples in which NO has been delivered to a target *in vivo* by a systemically administered nanostructure have not been reported.

Bottom-up supramolecular design of a targeted therapy requires integrating shape, targeting chemistry, and therapeutic functionalization. We have recently addressed shape and targeting using a peptide amphiphile (PA)-based delivery platform (39). PAs self-assemble into high-aspect ratio nanofibers in aqueous solutions (21) and have been investigated for applications in regenerative medicine, biomedical applications (10, 36), and systemic delivery (49). As a targeting moiety, we used a collagen IV-binding sequence that had previously been reported to successfully target nanoparticles to sites of vascular injury (5) and to deliver paclitaxel as a therapeutic agent (4). Incorporating this targeting chemistry in our PA-based platform, we recently showed specific binding to a site of arterial injury after systemic administration of targeted nanofibers (39).

With respect to NO functionalization, attention must be paid to developing a chemically stable NO-releasing nanostructure that will release NO upon entry into the bloodstream. Two forms of NO functionalization are most commonly used: diazeniumdiolation or S-nitrosylation. Each approach is associated with advantages and disadvantages. Diazeniumdiolates are donors that predictably release NO spontaneously upon exposure to hydrogen ions (24). S-nitrosothiols (RSNOs) release NO only when exposed to light or in the presence of certain agents, such as metal ions, reductants, or specific enzymes (50). Since many of these are present in the circulation, either chemistry can be used to design a therapy for intravascular use.

The advantage of S-nitrosylation chemistry is that it enables the creation of a stable NO-containing moiety without release of the signaling gas during synthesis of potential compounds. Moreover, RSNOs have direct biological activity independent of NO release (23, 50) and are implicated in vascular signaling and preservation of NO bioactivity (20, 32). We report here on the development and evaluation of a nanofiber built by self-assembly from a single molecule designed to carry NO *via* S-nitrosylation to the site of arterial injury through a simple, systemic intravenous injection. Concentration of the RSNO only to the site of vascular intervention avoids systemic side effects. Thus, we hypothesized that systemic administration of an NO-functionalized nanofiber targeted to collagen would durably prevent the development of neointimal hyperplasia.

## Results

### *Functionalization of targeted nanofibers*

To prevent the formation of neointimal hyperplasia, we functionalized the targeted PA nanofibers *via* S-nitrosylation of the cysteine residue (Fig. 1A). The formation of the S-nitrosyl (SNO) group leads to an absorbance peak around 350 nm, which allowed us to monitor the formation of the SNO nanofiber spectrophotometrically; the reaction was complete after 15 min (Fig. 1B). Additionally, the presence of thiols was monitored using Ellman's reagent, which indicated full loss of free thiols after S-nitrosylation (Fig. 1C).

The targeted SNO nanofiber was resolved by high-performance liquid chromatography (HPLC) (Fig. 1D) and electrospray ionization mass spectrometry (ESI-MS) (Fig. 1E) after S-nitrosylation. The mass spectrum shows an increase of 29 atomic units, which corresponds to the gain of an NO group and the loss of H. We characterized the supramolecular assembly of the SNO-targeted nanofiber *via* cryogenic transmission electron microscopy (cryo-TEM), which showed that the SNO-functionalized PA still forms nanofibers at neutral pH (Fig. 1F). This was confirmed by small-angle X-ray scattering (SAXS) analysis (Fig. 1G), where fits for a polydisperse core-shell yielded a shell thickness of 2.8 nm and a core radius of 1.2 nm. The fiber diameter is comparable with that of the non-S-nitrosylated targeted nanofiber (39).

### *SNO nanofiber* in vitro *response*

After showing functionalization of the targeted nanofibers, we characterized NO release, NO transfer, and cell response *in vitro*. Even though RSNOs are fairly stable in solution, they readily decompose in the presence of ascorbate and catalytic amounts of copper (Cu), releasing NO. The shift in absorbance spectrum was observed over time after addition of excess ascorbate and catalytic amounts of Cu(II), indicating decomposition of the SNO group (Fig. 2A). The absorbance kinetic trace showed pseudo-first-order decay with an apparent $t_{1/2}$ of 49 s at room temperature and pH 7.4 (Fig. 2B). To verify that the decomposition of the SNO group resulted in NO release in solution, we assessed nitrite by the Griess assay and NO *via* chemiluminescent detection. The Griess assay was performed to quantify nitrite ($NO_2^-$) release. Exposure of 60 $\mu$mol/L of SNO nanofiber to sodium ascorbate and Cu(II) resulted in 54 $\mu$mol/L of $NO_2^-$, which represents a 0.9 equiv release over 24 h (Fig. 2C).

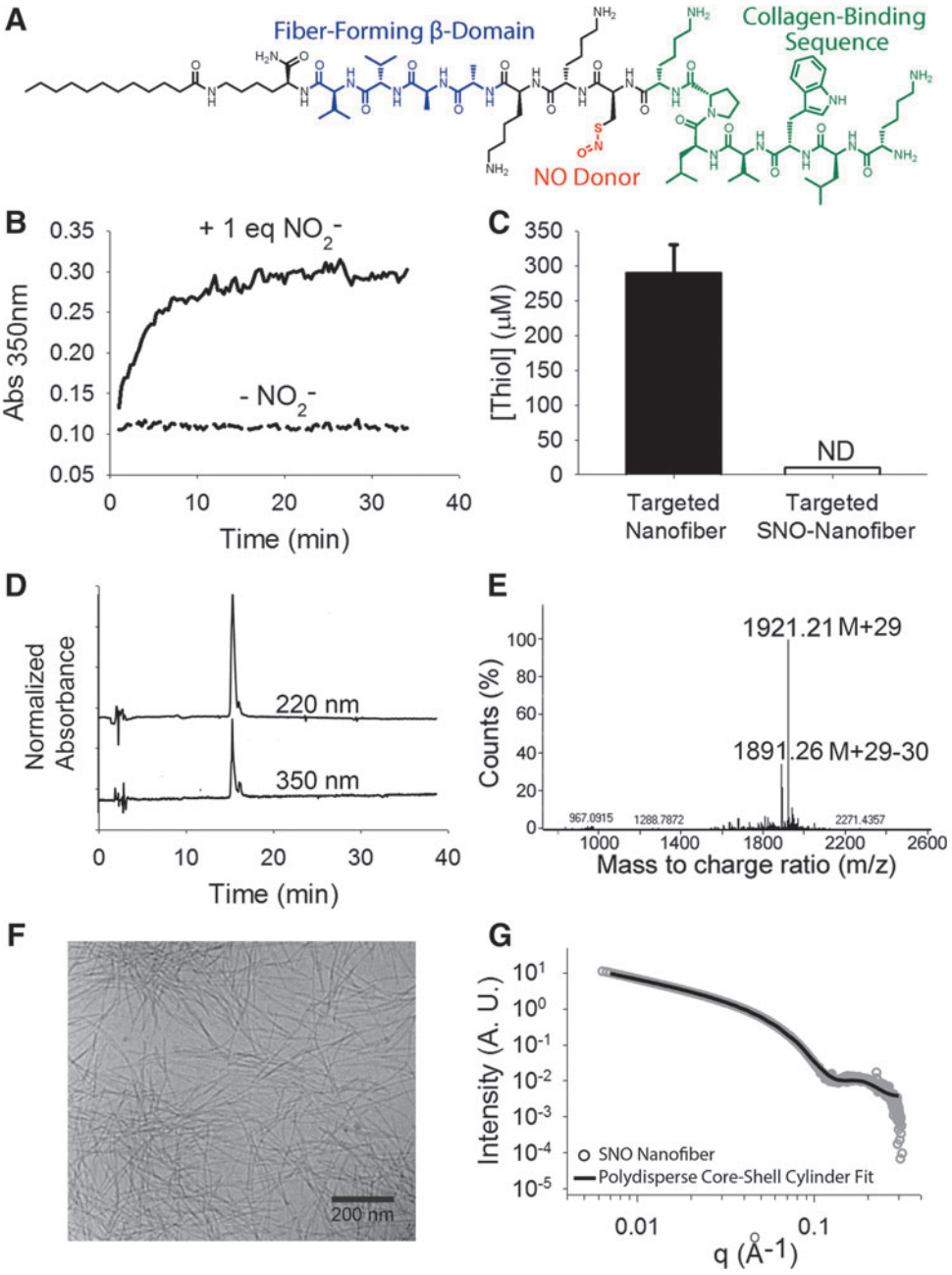


**FIG. 1. Synthesis and characterization of SNO-targeted peptide amphiphiles.** **(A)** Chemical structure of collagen-targeted S-nitroso (SNO) peptide amphiphile. **(B)** Kinetics of SNO formation when the targeted PA reacts with 1 equiv of $NaNO_2$. SNO formation corresponds to an increase in absorbance at 350 nm. **(C)** Ellman's test shows that all thiols are reacted after the addition of $NaNO_2$. **(D)** HPLC of SNO-targeted PA shows one large peak for normalized absorbances at both 220 and 350 nm (offset for clarity). **(E)** Deconvoluted mass spectrum showing the expected m/z after S-nitrosylation: M + 29 [mass of targeted nanofiber (1892) + mass of NO (30) − mass of hydrogen (1)]. **(F)** Cryogenic transmission electron microscopy of SNO nanofibers in phosphate-buffered saline, showing the high-aspect ratio fiber morphology. **(G)** SAXS yielding slopes of −1 in the low-q region, which suggests the presence of a cylindrical shape. Fit to a polydisperse core-shell yielded a shell thickness of 2.8 nm and a core radius of 1.2 nm. HPLC, high-performance liquid chromatography; ND, not determined; NO, nitric oxide; PA, peptide amphiphile; SAXS, small-angle X-ray scattering; SNO, S-nitrosyl. To see this illustration in color, the reader is referred to the web version of this article at www.liebertpub.com/ars

In the absence of ascorbate and Cu(II), there was little $NO_2^-$ accumulation over 24 h, in agreement with the expected stability of the SNO. As $NO_2^-$ is only an indirect measure of NO release, we confirmed this quantitative NO release using a chemiluminescent NO analyzer. In the presence of ascorbate and Cu(II), the S-nitrosylated targeted nanofiber released 90% of the theoretical yield (0.9 equi.) of NO (Fig. 2D). These findings were also confirmed with an ISO-NOPF 100 electrode to specifically detect NO in solution. In the presence of ascorbate and Cu(II), 5 $\mu M$ of SNO nanofibers quickly released NO with peak NO concentrations in a solution of $10^{-6}$ mol/L.

RSNOs can participate in transnitrosylation reactions by directly transferring the NO moiety to an acceptor thiol without release of NO. This reaction allows for the theoretical possibility that circulating plasma RSNOs can regenerate the SNO nanofibers, thereby replenishing the pool of available NO. To test if our targeted SNO nanofibers participate in S-nitrosylation reactions, we incubated targeted SH nanofibers with S-nitrosoglutathione (GSNO) and targeted SNO nanofibers with reduced glutathione (GSH). We followed the reactions by HPLC detecting GSH, GSNO, and the monomers, SH-PA and SNO-PA. In the presence of GSNO, SH-PA is converted to SNO-PA (Fig. 2E). Conversely, in the presence of GSH, the SNO-PA generates GSNO (Fig. 2F). At longer time points, other unidentified products appear, possibly disulfides or other thiol oxidation products.

Next, we assessed the effect of the targeted SNO nanofibers on vascular smooth muscle cell (VSMC) proliferation

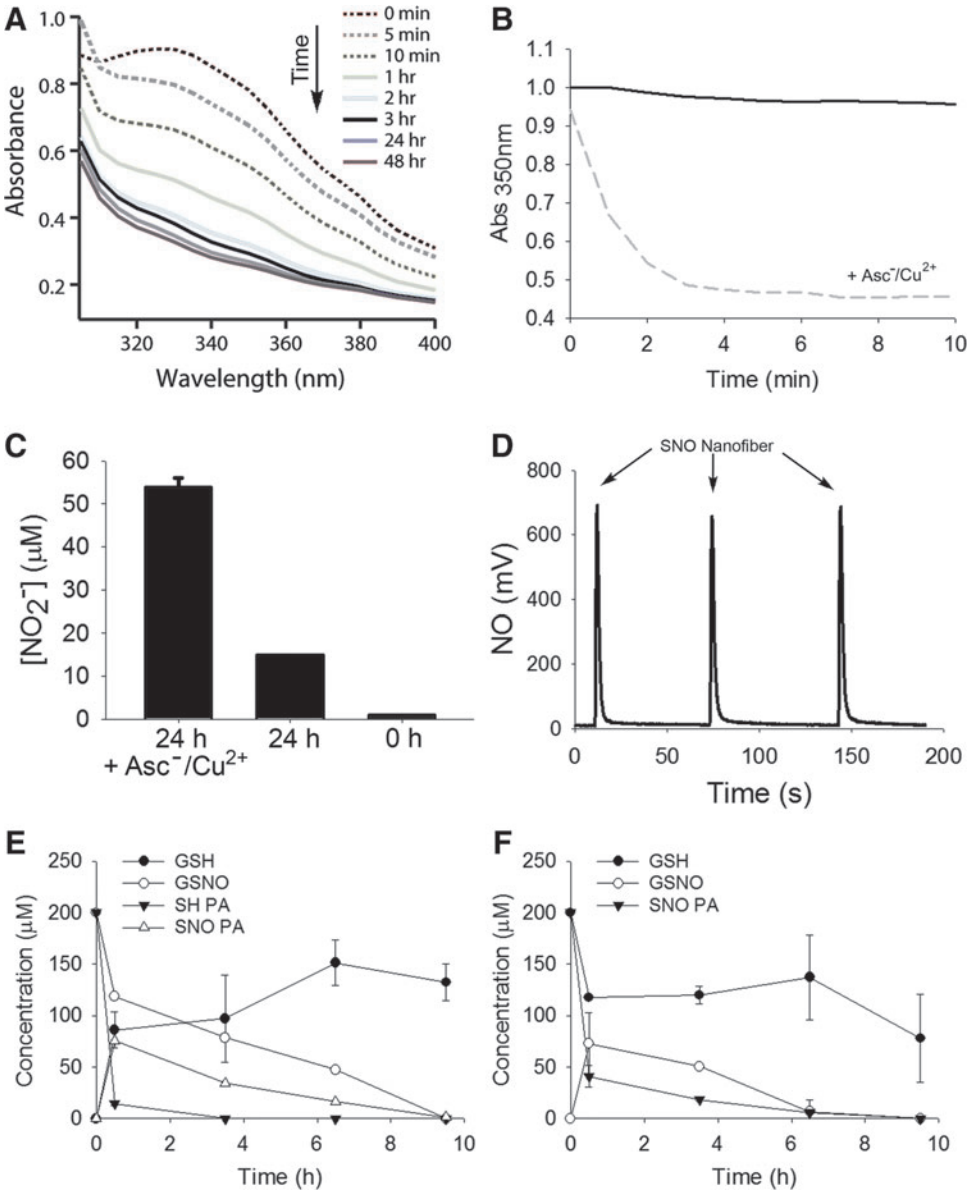


**FIG. 2.** ***In vitro*** **reactivity of SNO-targeted nanofibers. (A)** Absorbance spectrum of the SNO nanofibers (1 m*M*) with addition of ascorbate and $CuCl_2$ at 0, 5, and 10 min, and 1, 2, 3, 24, and 48 h. **(B)** SNO nanofiber (1 m*M*) stability in the absence of ascorbate and $CuCl_2$ (*black line*) and kinetic trace of decomposition of the SNO in the presence of ascorbate and $CuCl_2$ (*dashed gray line*) as evidenced by the absorbance change at 350 nm with an apparent $t_{1/2} = 49$ s at room temperature and pH 7.4. **(C)** Griess assay measurement after 24 h shows nitrite accumulation from the SNO nanofiber (60 $\mu M$) with the addition of ascorbate and copper. **(D)** NO chemiluminescent analyzer quantification of NO release from SNO nanofibers in the presence of ascorbate and $CuCl_2$. The *arrows* indicate the injection of the targeted SNO nanofiber (30 $\mu$l of 50 $\mu M$, 1.35 nmol). **(E)** Reaction between GSNO and SH-PA. GSNO and SH-PA at 200 $\mu$mol/L were allowed to react at 37°C and pH 7.4. Every 90 min an aliquot was analyzed by HPLC. The *open triangles* show the transient formation of SNO-PA. $N = 3$. **(F)** Reaction between SNO-PA and reduced GSH. GSH and SNO-PA at 200 $\mu$mol/L were allowed to react at 37°C and pH 7.4. Every 90 min an aliquot was analyzed by HPLC. The *open circles* show the transient formation of GSNO. $N = 3$. GSH, glutathione; GSNO, S-nitrosoglutathione.

and viability. VSMCs were treated with targeted nanofiber or targeted SNO nanofibers with and without ascorbate, copper, or a combination of ascorbate/copper. Up to 50 $\mu$mol/L, the SNO nanofiber itself did not have an effect on VSMC proliferation or total viable cell count (Fig. 3A, B). However, in the presence of 50 $\mu$mol/L ascorbate, 5 $\mu$mol/L copper, or a combination of both, 50 $\mu$mol/L of the SNO nanofiber significantly inhibited VSMC proliferation and total viable cell count (Fig. 3A, B). On the other hand, there was a significant increase in cell death with the SNO nanofiber with and without ascorbate and copper (Fig. 3C).

### *Localization of the targeted SNO nanofiber to the site of arterial injury*

To prove that S-nitrosylation does not prevent specific targeting, we investigated the binding of fluorescently tagged SNO nanofibers to balloon-injured carotid arteries. After

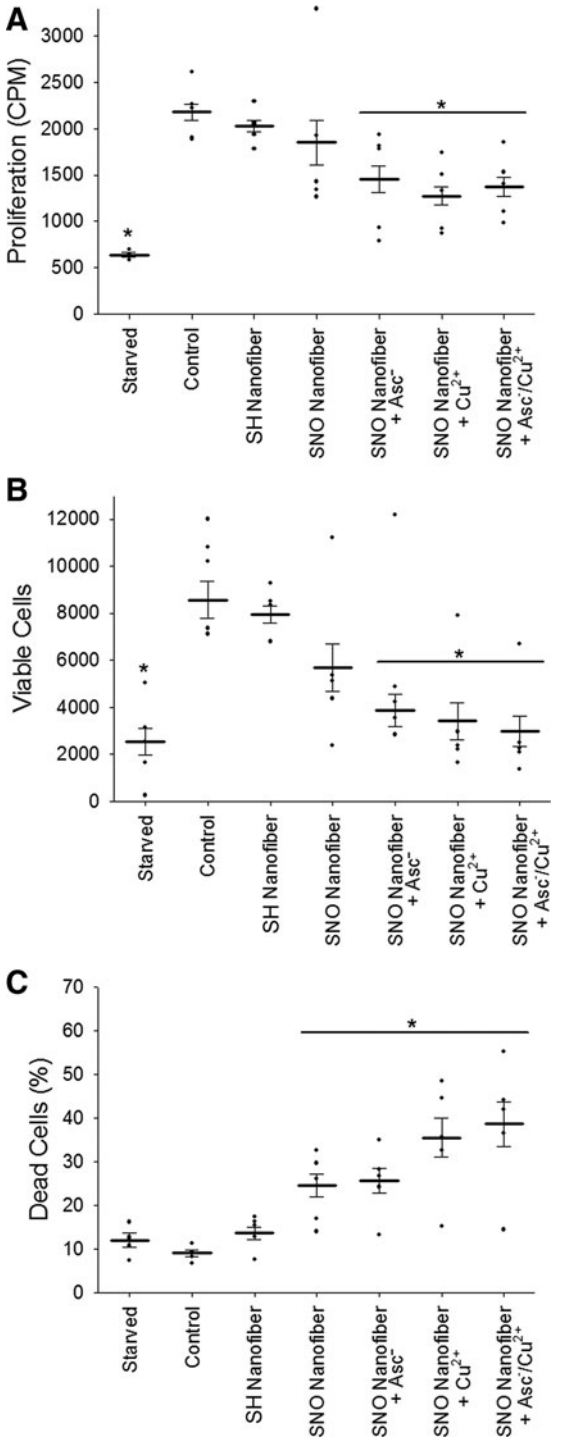


**FIG. 3. SNO-targeted nanofibers inhibit VSMC proliferation.** VSMCs were seeded onto 12-well plates at a density of 25,000 cells/well. Cells were allowed to adhere overnight, followed by serum starvation for 24 h to induce cell synchronization. **(A)** Proliferation after exposure to SNO nanofibers, with and without ascorbate (50 $\mu$mol/L), Cu(II) (5 $\mu$mol/L), and ascorbate/Cu(II), was measured by $^3$H-thymidine incorporation. $N=4$, $^*p<0.05$ compared with control. **(B)** Total viable cells and **(C)** percent dead cells were counted with the Muse benchtop cytometer. $N=5$, $^*p<0.05$ compared with control. VSMC, vascular smooth muscle cell.

injection of the fluorescently labeled SNO nanofibers, binding to the injured artery was detected by fluorescent microscopy (Fig. 4A, B). Targeted nanofiber binding to the luminal surface of the injured vessel was observed from 1 h up to 3 days; at day 5, binding was no longer detected (Fig. 4A, B). No binding was observed in the contralateral uninjured arteries (Fig. 4B). Whereas fluorescence is an indirect measurement, the presence of the fluorophore for 3 days at the site of injury suggests a local persistence of the nanofiber. The presence of the nanofiber at the site of arterial injury for 3 days is relevant since neointimal development in the rat carotid injury model proceeds with a peak in cell proliferation between days 2 and 4 (1, 9, 13).

To quantify the amount of the targeted SNO nanofiber that binds to the site of injury, we injected 2.5 mg of tagged SNO nanofiber after carotid artery balloon injury. After 1 h, we harvested the carotid and lysed the tissue. We analyzed the fluorescence recovered in the lysate compared with a known amount added to control uninjured arteries *ex vivo*. This method yielded an estimated 0.3 nmoles of SNO nanofiber bound to the site of injury. The balloon catheter used for the injury is 5 mm long, and the average diameter of the rat carotid artery is 0.71 mm (31), resulting in a total injured area of 11 mm$^2$. This represents a total binding density of the SNO nanofiber of 27 pmoles/mm$^2$, which is in excellent agreement with reported theoretical calculations for PA nanofibers covering a surface ($7\times10^{14}$ molecules/cm$^2$ equivalent to 10 pmoles/mm$^2$) (48).

### In vivo *biological activity of the SNO nanofiber*

We showed that the SNO nanofiber has antiproliferative effects *in vitro* and that it persists localized to the site of arterial injury *in vivo* for at least 3 days, a time period in which active cellular proliferation normally occurs following arterial injury. Hence, it was of interest to assess the effect of the targeted SNO nanofiber on actively proliferating cells *in vivo.* We determined the proliferative index by examining the percentage of cells that are bromodeoxyuridine (BrdU) positive in carotid artery sections 3 days after arterial injury. As expected, injured arteries had a higher proliferative index (ratio of BrdU-positive cells to total cellularity) compared with contralateral uninjured arteries (Fig. 5A, B). Treatment with the SNO nanofiber significantly reduced the proliferative index by 85% compared with nontreated, but injured, arteries (Fig. 5A, B, $p<0.05$).

We have previously shown that NO donors regulate cell proliferation and neointimal development by locally regulating the redox environment (3, 43). Thus, we hypothesized that the SNO nanofibers will change markers of NO-derived species at the site of arterial injury. To examine this hypothesis, we first assessed protein tyrosine nitration. Injured arteries showed increased tyrosine nitration compared with uninjured arteries (Fig. 5C, D, $p<0.05$). Interestingly, SNO nanofiber-treated animals showed a further increase in tyrosine nitration compared with injury alone (Fig. 5C, D, $p<0.05$).

These data suggest that the targeted SNO nanofiber is redox active at the site of arterial injury. To test if the SNO nanofiber is acting *via* release of NO or through direct SNO reactivity, we assessed local S-nitrosylation and local levels of cyclic guanosine monophosphate (cGMP). Injured arteries, with or without SNO nanofiber treatment, show similar levels of S-nitrosocysteine staining (Fig. 5E, F). To more

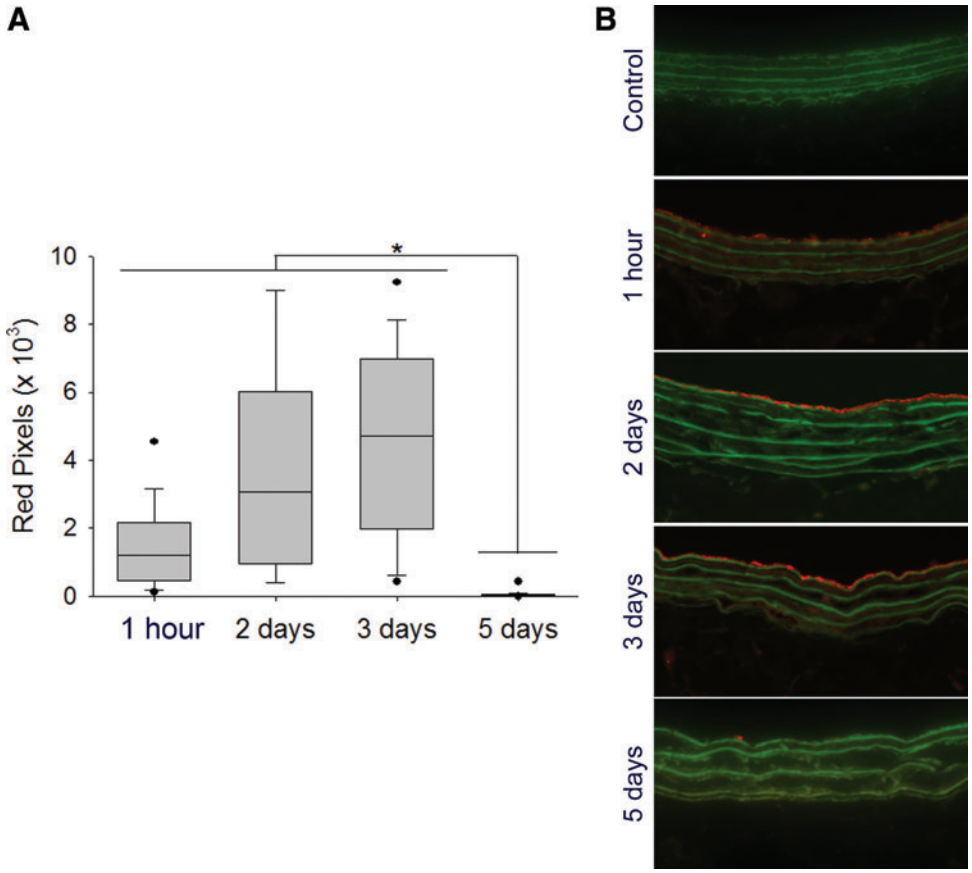


**FIG. 4. *In vivo* binding duration of the targeted SNO nanofibers.** The carotid artery balloon injury model was performed and 2.5 mg of Alexa-Fluor 546-tagged targeted SNO nanofiber was injected *via* the tail vein. At different time points, the carotid arteries were harvested and binding of the nanofiber to the injured artery was assessed *via* fluorescent microscopy using a 20× objective. **(A)** Red pixel quantification of bound nanofiber. The fluorescence persists at the site of interest until day 3. $N = 2$ rats/group with 15 technical replicates, $^*p < 0.05$. **(B)** Representative cross-section fluorescence imaging of control and injured carotid arteries from animals injected with the targeted nanofiber (2.5 mg) over time. *Red* = Alexa Fluor tag, *Green* = elastic lamina. To see this illustration in color, the reader is referred to the web version of this article at www.liebertpub.com/ars

specifically assess levels of S-nitrosylated proteins, we performed a biotin-switch assay on carotid lysates harvested 2 h after balloon injury and administration of 2.5 mg of targeted SNO nanofibers. The S-nitrosylated proteins were below the level of detection for injured and control arteries. To evaluate the levels of cGMP in the artery, injured and contralateral uninjured carotids were harvested 2 h after surgery and SNO nanofiber administration. There were no significant differences between the treatment group and the control (control group = 3.1 ± 2.5 pmol/mg protein, and SNO nanofiber group = 1.2 ± 0.3 pmol/mg protein, $N = 3$, $p$ = NS).

### *Inhibition of neointimal hyperplasia by the targeted SNO nanofiber*

Next, we determined the *in vivo* effect of the targeted SNO nanofiber on neointimal hyperplasia using the rat carotid artery balloon injury model. Evaluation of arterial cross sections showed that injury alone caused neointimal hyperplasia after 2 weeks (Fig. 6A–C). Similar levels of neointimal hyperplasia were observed with the nontargeted nanofiber, the nontargeted SNO nanofiber, and the targeted nanofiber. Interestingly, only the targeted SNO nanofiber inhibited the development of neointimal hyperplasia upon evaluation of multiple metrics (Fig. 6A–C). There was a 55% reduction in the intima/media (I/M) area ratio and a 41% reduction in percent occlusion with the targeted SNO nanofiber group compared with injury alone ($p < 0.01$, Fig. 6B, C).

Another important observation is that the targeted SNO nanofiber significantly inhibited neointimal hyperplasia compared with both the nontargeted SNO nanofiber and the targeted nanofiber without SNO functionalization. Compared with the nontargeted SNO nanofiber, the targeted SNO nanofiber inhibited the I/M area ratio by 46% ($p = 0.047$) and percent occlusion by 56% ($p < 0.001$, Fig. 6B, C). Compared with the targeted nanofiber without NO functionalization, the targeted SNO nanofiber inhibited the percent occlusion by 46% ($p < 0.001$, Fig. 6B, C). No differences were observed in the I/M area ratio and percent occlusion between the no treatment, targeted nanofiber, and nontargeted SNO nanofiber. Together, these data indicate that the integration of the collagen-binding sequence for targeting and the SNO functionalization into a filamentous supramolecular vehicle are essential for a therapeutic effect.

Next, we evaluated whether these nanofiber constructs induced inflammation in the vasculature. Evaluation of arterial sections using immunofluorescence staining with an antibody for ED1, a marker for macrophages, revealed no differences between the five treatment groups at 2 weeks (Fig. 6D, E).

To determine if the targeted SNO nanofiber effected reendothelialization of the injured artery, we measured the area of denudation remaining 3 days after injury using Evans Blue dye injection. We found no differences in the injured area between the different treatment groups at 3 days (Evans Blue area in injury alone = 8.7 ± 0.9 $mm^2$ *vs.* SNO nanofiber treated = 8.5 ± 0.7 $mm^2$, $N = 3$, $p$ = NS). This is not surprising as 3 days might be too early to assess reendothelialization.

Last, we investigated if the inhibition of neointimal hyperplasia achieved with the targeted SNO nanofiber was

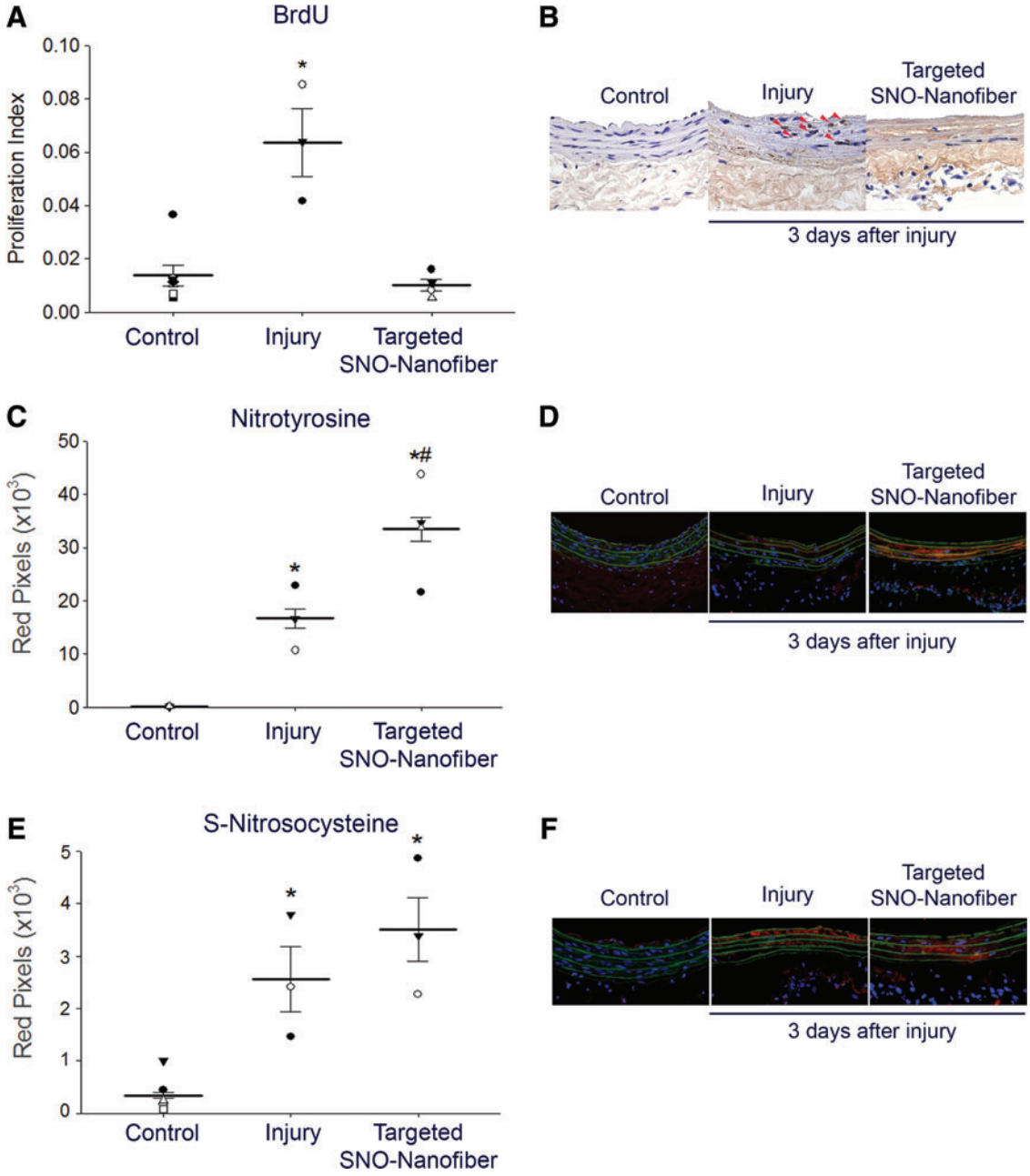


**FIG. 5.** ***In vivo*** **local effect of targeted SNO nanofibers on the vascular wall.** The carotid artery balloon injury model was performed with or without tail vein administration of 2.5 mg targeted SNO nanofiber. At 24 and 1 h before sacrifice, a bromodeoxyuridine (BrdU) solution (100 mg/ml) was administered *via* intraperitoneal injection to label rapidly proliferating cells. At 3 days, carotid arteries were harvested for analysis. **(A)** Proliferative index (ratio of BrdU+ cells over total cells). $N=3$ for injury alone, $N=4$ for targeted SNO nanofiber, and $N=7$ for uninjured control. Each data point represents one rat as the average of 10–20 technical replicates. $^{*}p<0.05$ compared with control and targeted SNO nanofibers. **(B)** Representative cross sections of the immunohistochemical staining using a 20× objective. *Red arrowheads* show BrdU-positive cells. **(C)** Immunofluorescence quantification for nitrotyrosine staining. $N=3$ for injury alone, $N=4$ for targeted SNO nanofiber, and $N=4$ for uninjured control. Each data point represents one rat as the average of 10–20 technical replicates. $^{*}p<0.05$ compared with control and $^{\#}p<0.05$ compared with injury alone. **(D)** Representative cross sections of immunofluorescence staining for nitrotyrosine (*red*) using a 20× objective. *Green* = elastic lamina; *blue* = nuclei. **(E)** Immunofluorescence quantification for S-nitrosocysteine staining. $N=3$ for injury alone, $N=4$ for targeted SNO nanofiber, and $N=7$ for uninjured control. Each data point represents one rat as the average of 10–20 technical replicates. $^{*}p<0.05$ compared with control. **(F)** Representative cross sections of immunofluorescence staining for S-nitrosocysteine (*red*) using a 20× objective. *Green* = elastic lamina; *blue* = nuclei. To see this illustration in color, the reader is referred to the web version of this article at www.liebertpub.com/ars

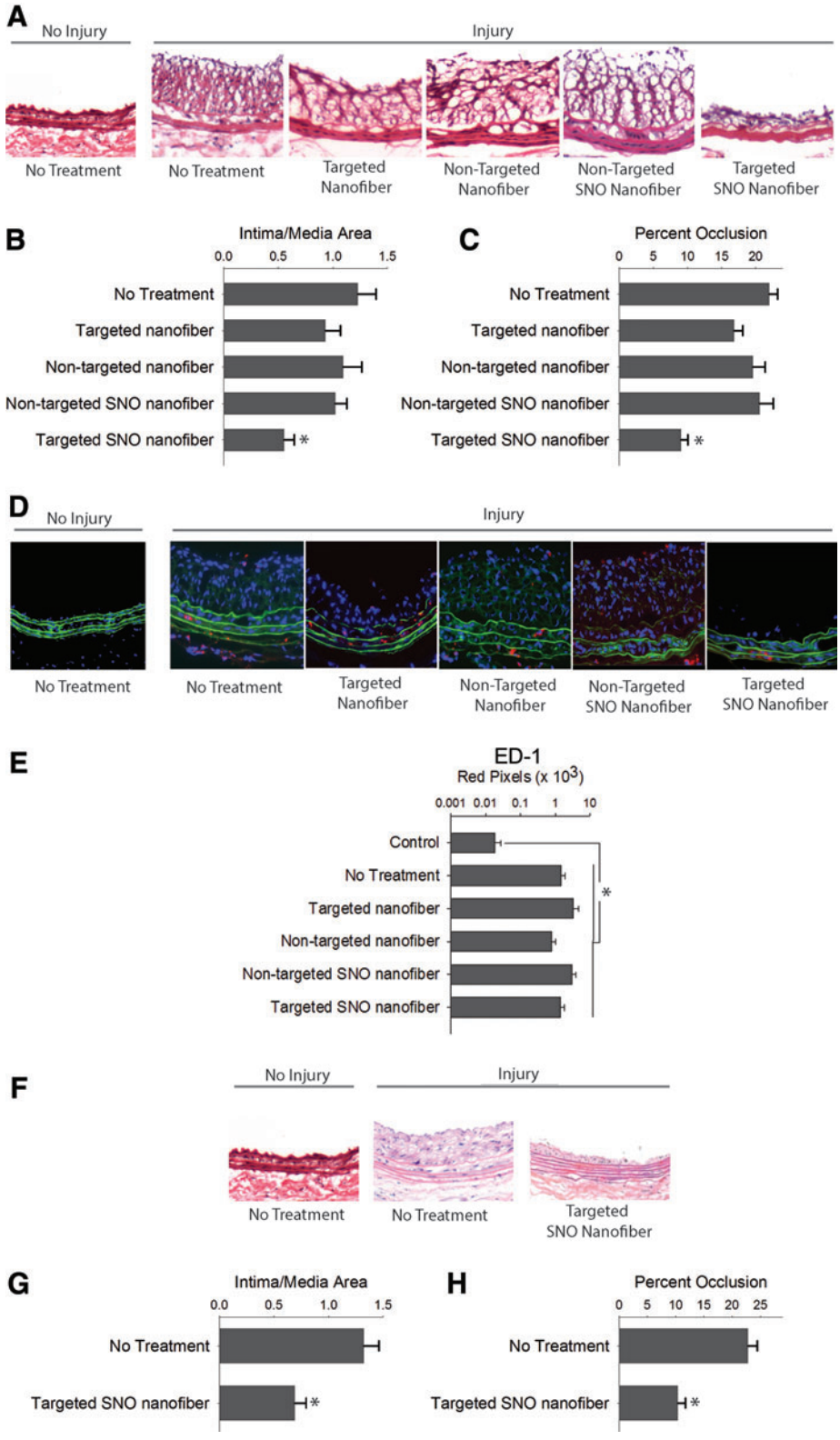


**FIG. 6. Targeted SNO nanofibers inhibit neointimal hyperplasia. (A)** Arterial cross sections of carotid arteries 2 weeks after balloon injury using a 20× objective. **(B)** The targeted SNO nanofiber (0.5 mg) inhibited the intima-to-media area ratio by 55% *versus* no treatment ($*p < 0.05$ *vs.* no treatment, targeted nanofibers, and targeted SNO nanofibers). **(C)** The targeted SNO nanofiber decreased percent occlusion by 41% *versus* no treatment ($*p < 0.05$ *vs.* no treatment, targeted nanofibers, and targeted SNO nanofibers). $N = 6$/treatment group. **(D)** Representative images of immunofluorescence staining of macrophages (*red*) using a 20× objective. *Green* = elastic lamina; *blue* = nuclei. **(E)** Quantification of ED1-positive staining. $N = 4$–7/treatment group, $*p < 0.05$ compared with uninjured control. **(F)** The targeted SNO nanofiber (5 mg) continued to inhibit neointimal hyperplasia for 7 months. Representative hematoxylin and eosin-stained arterial cross sections of carotid arteries 7 months after balloon injury using a 20× objective. **(G)** Intima-to-media area ratio decreased 51% with the targeted S-nitrosothiol (SNO) nanofiber compared with control ($*p < 0.001$). $N = 7$/treatment group. **(H)** Percent occlusion decreased 45% with the targeted SNO nanofiber compared with control ($*p = 0.001$). $N = 7$/treatment group. To see this illustration in color, the reader is referred to the web version of this article at www.liebertpub.com/ars

durable. Importantly, we found that a single injection of the targeted SNO nanofiber at the time of injury continued to inhibit neointimal hyperplasia up to 7 months following arterial balloon injury (Fig. 6F–H), causing a 51% decrease in the I/M area ratio ($p < 0.05$) and a 45% reduction in percent occlusion ($p < 0.05$) compared with injury alone (Fig. 6G, H).

### *Systemic effects of the targeted SNO nanofiber*

After showing efficacy inhibiting neointimal hyperplasia, we sought to assess the systemic effects of the targeted SNO nanofiber. First, we assessed for complement activation by the SNO nanofiber. A functional complement activity assay

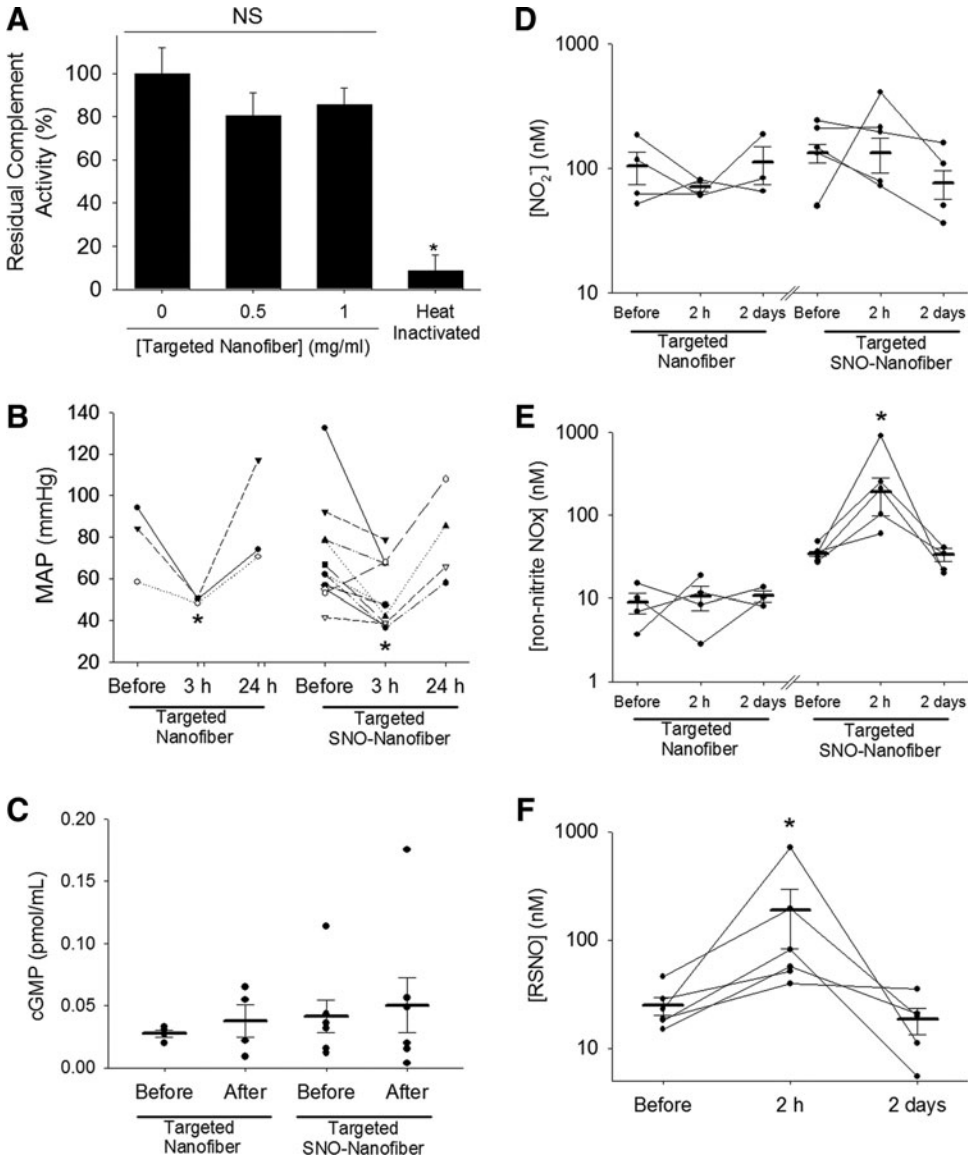


**FIG. 7. Systemic effects of the targeted SNO nanofibers. (A)** Functional complement activation assay shows that the targeted SNO nanofibers do not activate the complement in human serum *ex vivo.* Residual compliment activity was measured after incubation with and without targeted nanofibers. Total depletion was achieved by heat inactivation of serum as a control. $N=3$, $^*p<0.05$ versus nonheat treated. NS, nonsignificant. **(B)** MAP was measured before surgery and 3 h and 24 h after surgery and administration of 2.5 mg of either the targeted nanofiber or the targeted SNO nanofiber. $N=3$ for targeted nanofiber, $N=4$–10 for the targeted SNO nanofiber. $^*p<0.05$ with respect to MAP before surgery. **(C)** cGMP levels were measured in plasma before surgery and 2 hours after surgery and administration of 2.5 mg of either the targeted nanofiber or the targeted SNO nanofiber. $N=4$ for targeted nanofiber, $N=6$ for targeted SNO nanofiber. $p=$NS. Plasma reactive nitrogen species (NOx) were measured for **(D)** nitrite levels, **(E)** non-nitrite NOx, and **(F)** RSNO. Blood was collected before surgery and 2 h and 2 days after surgery and administration of 2.5 mg of either the targeted nanofiber or the targeted SNO nanofiber *via* chemiluminescent detection. $N=3$–4 for targeted nanofiber, $N=4$–5 for the targeted SNO nanofiber. $^*p<0.05$ with respect to levels before surgery. cGMP, cyclic guanosine monophosphate; MAP, mean arterial pressure.

revealed that the targeted SNO nanofiber did not activate the complement system in human serum *ex vivo* at doses of 0.5 mg/ml and 1.0 mg/ml (Fig. 7A). Total depletion of complement activity was achieved by heat inactivation of serum. The residual complement activity of nontreated control serum was $100\pm12\%$, serum treated with the targeted SNO nanofiber at a dose of 0.5 mg/ml was $81\pm11\%$, and serum treated with the targeted SNO nanofiber at a dose of 1.0 mg/ml was $86\pm8\%$ (Fig. 7A).

Next, we evaluated the blood pressure of animals immediately before surgery, 3 h and 24 h after surgery, administration of either 2.5 mg of targeted nanofiber or targeted SNO nanofibers. The mean arterial pressure (MAP) dropped from $83\pm9$ mmHg to $64\pm11$ mmHg in the targeted nanofiber-treated rats ($p<0.05$) and from $71\pm8$ mmHg to $52\pm5$ mmHg in the targeted SNO nanofiber-treated rats ($p<0.05$, Fig. 7B). The MAP of both groups returned to normal after 24 h (Fig. 7B). Surgery alone did not cause a drop in MAP. This

suggests that the nanofibers cause a transient drop in the MAP that is independent of surgery and, most importantly, independent of the presence of the SNO group.

To further investigate if significant levels of NO are released in the circulation, we evaluated plasma levels of cGMP. Blood was collected from the tail vein of rats immediately before surgery and 2 h after surgery and administration of either the targeted nanofiber or the targeted SNO nanofiber. There was no significant increase in plasma levels of cGMP (Fig. 7C). Because the preceding techniques may not accurately capture the effects of systemic NO release due to a number of factors—including timing of our collection points and degradation of cGMP—we assessed levels of NO species (NOx) in the plasma using a Sievers NO analyzer. Following the method described by MacArthur *et al.* (33), we used the triiodide method to measure total NOx. To identify different species, we used sulfanilamide to block the $NO_2^-$ signal and $HgCl_2$ to block the signal from RSNO.

Administration of the targeted nanofiber with or without SNO did not cause a change in plasma $NO_2^-$ (Fig. 7D). However, there was a significant increase in non-nitrite NOx at 2 h in plasma of rats that received the targeted SNO nanofiber (Fig. 7E). Levels returned to baseline after 2 days (Fig. 7E). To further characterize this increase of NOx, we blocked the RSNO signal with Hg. We determined that most of the non-nitrite signal was due to a significant increase in RSNO from basal levels of 25 to 189 $\mu$mol/L ($p < 0.05$) at 2 h after surgery (Fig. 7F). Levels returned to normal (18 $\mu$mol/L) after 2 days. This suggests the possibility that the targeted SNO nanofibers increase plasma RSNO *via* transnitrosylation reactions.

Finally, blood samples were collected up to 1 week after injection of the targeted nanofibers or the targeted SNO nanofibers for hematological, coagulation, and clinical chemistry analyses. Hematology data are shown in Tables 1 and 2 and coagulation data are shown in Tables 3 and 4. Both targeted nanofibers caused a transient shift in the leukocyte differential, with an increase in the percentage of segmented neutrophils and a decrease in the percentage of lymphocytes at 3 h postinjection (Tables 1 and 2, $p < 0.05$). The values returned to normal after 1 day. No other hematology or coagulation variable was affected by the SNO nanofiber. A transient decrease in the white blood cell count was observed in the targeted SH nanofiber-treated animals at day 1, but returned to normal by day 3 (Table 2).

Regarding the clinical chemistry data, the targeted SH and SNO nanofibers induced a two-fold increase in blood urea nitrogen (BUN) at 3 h after injection (Tables 3 and 4, $p < 0.05$). This increase returned to baseline after 1 day. There was a trend towards an increase in creatinine at 3 h after injection that was not statistically significant compared with our controls (Tables 3 and 4). The targeted SH and SNO nanofiber also induced a transient increase in plasma creatine kinase (CK) and glucose at 3 h after injection, but returned to baseline after 1 day (Tables 3 and 4, $p < 0.05$). There was a trend towards an increase in plasma aspartate transaminase at 3 h after injection that was not statistically significant compared with our controls (Tables 3 and 4).

Finally, there was a statistically significant decrease in plasma alanine transaminase levels compared with control, which persisted at all the time points evaluated only in SNO nanofiber-treated animals. However, these values are within the normal range compared with reference data, so this decrease was not considered clinically significant (37). In conclusion, both the SNO and non-SNO-targeted nanofibers showed similar patterns in hematological and blood chemistry parameters, suggesting that the transient effects observed are not dependent on the presence of the SNO moiety.

Table 1. Hematology and Coagulation Panel for Targeted S-Nitrosyl Nanofiber

| | | | *Targeted SNO nanofiber* | | | | | | | | | |
|---|---|---|---|---|---|---|---|---|---|---|---|---|
| | *Control group* | | *3 h* | | *Day 1* | | *Day 2* | | *Day 3* | | *Day 7* | |
| | *Mean* | *SEM* | *Mean* | *SEM* | *Mean* | *SEM* | *Mean* | *SEM* | *Mean* | *SEM* | *Mean* | *SEM* |
| Hematology | | | | | | | | | | | | |
| White blood cells ($10^3/\mu$l) | 6.5 | ±1.6 | 7.8 | ±0.6 | 5.4 | ±0.9 | 6.1 | ±1.0 | 4.1 | ±0.4 | 6.3 | ±1.3 |
| Red blood cells ($10^6/\mu$l) | 7.3 | ±0.6 | 9.4 | ±0.2 | 7.5 | ±0.4 | 7.7 | ±0.1 | 8.0 | ±0.2 | 7.6 | ±0.2 |
| Hemoglobin (g/dl) | 13.9 | ±1.1 | 17.4 | ±0.5 | 13.7 | ±0.6 | 14.2 | ±0.6 | 14.8 | ±0.5 | 14.0 | ±0.3 |
| Mean corpuscular volume (fl) | 55.7 | ±0.6 | 52.8 | ±1.0 | 52.8 | ±0.5 | 54.0 | ±1.0 | 53.7 | ±0.3 | 53.3 | ±0.9 |
| Differential (%) | | | | | | | | | | | | |
| Segmented Neutrophils | 23.3 | ±5.2 | **58.1*** | **±3.6** | 20.6 | ±1.6 | 15.3 | ±2.4 | 13.8 | ±3.7 | 13.8 | ±0.2 |
| Lymphocytes | 72.3 | ±5.4 | **36.2*** | **±4.7** | 75.7 | ±1.7 | 79.8 | ±2.5 | 82.5 | ±3.3 | 82.4 | ±0.4 |
| Monocytes | 2.5 | ±0.3 | 4.9 | ±1.1 | 1.9 | ±0.2 | 2.5 | ±0.1 | 2.4 | ±0.6 | 1.6 | ±0.3 |
| Eosinophils | 1.4 | ±0.3 | 0.6 | ±0.3 | 1.2 | ±0.1 | 1.6 | ±0.3 | 1.6 | ±0.3 | 1.6 | ±0.1 |
| Basophils | 0.13 | ±0.04 | 0.15 | ±0.08 | 0.10 | ±0.03 | 0.17 | ±0.07 | 0.13 | ±0.03 | 0.23 | ±0.03 |
| Coagulation panel | | | | | | | | | | | | |
| Platelet count ($10^3/\mu$l) | 544 | ±120 | 549 | ±91 | 984 | ±59 | 906 | ±81 | 830 | ±79 | 902 | ±45 |
| Prothrombin time (s) | 18.2 | ±2.4 | 18.1 | ±1.2 | 24.1 | ±6.4 | 14.7 | ±0.3 | 17.3 | ±0.3 | 21.6 | ±1.9 |
| Partial thromboplastin time (s) | 52 | ±4 | 57 | ±5 | 57 | ±10 | 43 | ±2 | 38 | ±4 | 68 | ±10 |

Bold denotes statistical significance.
*$p < 0.05$ with respect to the control group. $N = 3$–6 animals per group.
SEM, standard error of the mean; SNO, S-nitrosyl.

Table 2. Hematology and Coagulation Panel for Targeted SH Nanofiber

| | *Control group* | | *Targeted SH nanofiber* | | | | | | | | | |
|---|---|---|---|---|---|---|---|---|---|---|---|---|
| | | | *3 h* | | *Day 1* | | *Day 2* | | Day 3 | | Day 7 | |
| | *Mean* | *SEM* | *Mean* | *SEM* | *Mean* | *SEM* | *Mean* | *SEM* | *Mean* | *SEM* | *Mean* | *SEM* |
| Hematology | | | | | | | | | | | | |
| White blood cells ($10^3/\mu l$) | 6.5 | ±1.6 | 6 | ±2 | **3.5*** | **±0.5** | **3.5*** | **±1** | 5.5 | ±0.6 | 3.8 | ±0.8 |
| Red blood cells ($10^6/\mu l$) | 7.3 | ±0.6 | 7.1 | ±0.4 | 7.4 | ±0.5 | 6.5 | ±0.6 | 7.8 | ±0.2 | 5.4 | ±0.9 |
| Hemoglobin (g/dl) | 13.9 | ±1.1 | 13.1 | ±0.7 | 13.9 | ±0.8 | 12 | ±1 | 14.6 | ±0.2 | 10.1 | ±1.5 |
| Mean corpuscular volume (fl) | 55.7 | ±0.6 | 54.6 | ±0.9 | 54.5 | ±0.7 | 54 | ±1 | 55 | ±1 | 52.7 | ±1.2 |
| Differential (%) | | | | | | | | | | | | |
| Segmented Neutrophils | 23.3 | ±5.2 | **51*** | **±7** | 26 | ±3 | 21 | ±4 | 25 | ±2 | 10.2 | ±1.1 |
| Lymphocytes | 72.3 | ±5.4 | **44*** | **±8** | 70 | ±3 | 75 | ±4 | 70 | ±3 | 86.4 | ±1.4 |
| Monocytes | 2.5 | ±0.3 | 2.3 | ±0.4 | 2.4 | ±0.4 | 2.1 | ±0.2 | 2 | ±0.4 | 1.3 | ±0.2 |
| Eosinophils | 1.4 | ±0.3 | 1.8 | ±0.4 | 1.6 | ±0.4 | 1.3 | ±0.2 | 2.2 | ±0.4 | 1.43 | ±0.03 |
| Basophils | 0.13 | ±0.04 | 0.20 | ±0.06 | 0.20 | ±0.03 | 0.10 | ±0.02 | 0.10 | ±0.02 | 0.17 | ±0.12 |
| Coagulation panel | | | | | | | | | | | | |
| Platelet count ($10^3/\mu l$) | 544 | ±120 | 532 | ±183 | 473 | ±72 | 355 | ±105 | 576 | ±89 | 291 | ±226 |
| Prothrombin time (s) | 18.2 | ±2.4 | 23.5 | ±8.0 | 22.2 | ±4.1 | 20.6 | ±0.1 | 14.3 | ±0.2 | 32.8 | ±17.5 |
| Partial thromboplastin time (s) | 52 | ±4 | 51 | ±4 | 47 | ±3 | 50 | ±1 | 55 | ±2 | 55 | ±9 |

*$p < 0.05$ with respect to the control group. $N = 3$–6 animals per group. Bold denotes statistical significance.

## Discussion

We describe here the development and evaluation of a supramolecular nanofiber that delivers NO *via* systemic intravenous injection, but targets the SNO nanofiber to the specific site of arterial intervention to prevent neointimal hyperplasia. This novel modality incorporating targeting and therapeutic chemistries with a supramolecular delivery platform was able to exert the desired biological effect while overcoming some of the challenges posed by NO-based therapies. This therapy has great potential for clinical use in the vasculature and beyond given its simplicity, efficacy, ability to redose, and apparent safety.

Targeted delivery of a cancer chemotherapeutic agent, paclitaxel, with lipid-polymeric nanoparticles to prevent neointimal hyperplasia has been reported using the same targeting peptide sequence (4). However, paclitaxel is an indiscriminate inhibitor of cellular proliferation and inhibits endothelial cell proliferation, which is detrimental to vasculature health. Moreover, paclitaxel-eluting stents are associated with a higher risk of late in-stent thrombosis compared with bare metal stents (41, 51). The use of a therapeutic agent

Table 3. Clinical Chemistry Panel for Targeted S-Nitrosyl Nanofiber

| | *Control group* | | *Targeted SNO nanofiber* | | | | | | | | | |
|---|---|---|---|---|---|---|---|---|---|---|---|---|
| | | | *3 h* | | *Day 1* | | *Day 2* | | *Day 3* | | *Day 7* | |
| | *Mean* | *SEM* | *Mean* | *SEM* | *Mean* | *SEM* | *Mean* | *SEM* | *Mean* | *SEM* | *Mean* | *SEM* |
| Alkaline phosphatase (U/L) | 185 | ±19 | 153 | ±13 | 229 | ±20 | 196 | ±31 | 144 | ±8 | 203 | ±15 |
| Alanine transaminase (U/L) | 94 | ±13 | **58*** | **±2** | **58*** | **±6** | **48*** | **±3** | **42*** | **±5** | **51*** | **±3** |
| Aspartate transaminase (U/L) | 145 | ±27 | 162 | ±31 | 98 | ±15 | 64 | ±5 | 54 | ±5 | 69 | ±9 |
| Creatine kinase (U/L) | 565 | ±118 | **452*** | **±44** | 175 | ±12 | 231 | ±36 | 145 | ±2 | 237 | ±67 |
| Total protein (g/dl) | 5.5 | ±0.1 | 4.9 | ±0.1 | 5.7 | ±0.1 | 5.4 | ±0.1 | 5.7 | ±0.1 | 5.5 | ±0.1 |
| Albumin (g/dl) | 2.9 | ±0.1 | 2.6 | ±0.1 | 2.9 | ±0.0 | 2.8 | ±0.0 | 2.9 | ±0.1 | 2.8 | ±0.1 |
| Globulin (g/dl) | 2.6 | ±0.1 | 2.3 | ±0.1 | 2.8 | ±0.1 | 2.6 | ±0.1 | 2.8 | ±0.1 | 2.7 | ±0.1 |
| Blood urea nitrogen (mg/dl) | 18 | ±1 | **33.5*** | **±1.5** | 21.8 | ±1.1 | 17.0 | ±1.7 | 19.7 | ±0.7 | 23.3 | ±2.4 |
| Creatinine (mg/dl) | 0.38 | ±0.02 | 0.7 | ±0.1 | 0.4 | ±0.0 | 0.4 | ±0.0 | 0.4 | ±0.0 | 0.4 | ±0.0 |
| Cholesterol (mg/dl) | 86.5 | ±4.5 | 67.2 | ±1.7 | 85.5 | ±2.5 | 95.3 | ±5.7 | 91.7 | ±2.7 | 78.7 | ±0.3 |
| Glucose (mg/dl) | 259 | ±17 | **413*** | **±29** | 250 | ±9 | 256 | ±9 | 275 | ±7 | 297 | ±25 |
| Phosphate (mg/dl) | 7.3 | ±0.2 | 10.2 | ±0.9 | 7.9 | ±0.1 | 7.4 | ±0.1 | 7.4 | ±0.2 | 8.4 | ±0.9 |
| Bicarbonate (mmol/L) | 25.8 | ±0.5 | 19 | ±1 | 24 | ±1 | 24.3 | ±0.3 | 23 | ±0.6 | 25 | ±1 |
| Sodium (mmol/L) | 142.0 | ±0.4 | 137.8 | ±1.2 | 142.3 | ±0.3 | 141.0 | ±0.3 | 140.7 | ±0.6 | 140.3 | ±1.3 |
| Potassium (mmol/L) | 4.6 | ±0.1 | 5.7 | ±0.2 | 5.2 | ±0.1 | 5.2 | ±0.1 | 5.2 | ±0.1 | 5.2 | ±0.3 |

*$p < 0.05$ with respect to the control group. $N = 3$–6 animals per group. Bold denotes statistical significance.

Table 4. Clinical Chemistry Panel for Targeted SH Nanofiber

| | *Control group* | | *Targeted SH nanofiber* | | | | | | | | | |
|---|---|---|---|---|---|---|---|---|---|---|---|---|
| | | | *3 h* | | *Day 1* | | *Day 2* | | *Day 3* | | *Day 7* | |
| | *Mean* | *SEM* | *Mean* | *SEM* | *Mean* | *SEM* | *Mean* | *SEM* | *Mean* | *SEM* | *Mean* | *SEM* |
| Alkaline phosphatase (U/L) | 185 | ±19 | 162 | ±10 | 154 | ±17 | 183 | ±7 | 179 | ±12 | 180 | ±12 |
| Alanine transaminase (U/L) | 94 | ±13 | 177 | ±128 | 117 | ±51 | 61 | ±4 | 46 | ±3 | 72 | ±3 |
| Aspartate transaminase (U/L) | 145 | ±27 | 287 | ±135 | 164 | ±67 | 73 | ±6 | 75 | ±8 | 96 | ±7 |
| Creatine kinase (U/L) | 565 | ±118 | **2412*** | **±1517** | 335 | ±34 | 251 | ±46 | 294 | ±81 | 378 | ±58 |
| Total protein (g/dl) | 5.5 | ±0.1 | 4.9 | ±0.2 | 5.4 | ±0.1 | 5.5 | ±0.1 | 5.6 | ±0.1 | 5.7 | ±0.1 |
| Albumin (g/dl) | 2.9 | ±0.1 | 2.5 | ±0.1 | 2.9 | ±0.1 | 2.9 | ±0.1 | 3.0 | ±0.1 | 2.9 | ±0.0 |
| Globulin (g/dl) | 2.6 | ±0.1 | 2.4 | ±0.1 | 2.5 | ±0.1 | 2.6 | ±0.1 | 2.7 | ±0.1 | 2.9 | ±0.1 |
| Blood urea nitrogen (mg/dl) | 18 | ±1 | **37*** | **±2** | 21 | ±2 | 19 | ±1 | 20 | ±1 | 20 | ±1 |
| Creatinine (mg/dl) | 0.38 | ±0.02 | 1.02 | ±0.18 | 0.40 | ±0.02 | 0.40 | ±0.02 | 0.40 | ±0.02 | 0.40 | ±0.00 |
| Cholesterol (mg/dl) | 86.5 | ±4.5 | 70 | ±8 | 81 | ±3 | 85 | ±3 | 97 | ±3 | 87.3 | ±0.9 |
| Glucose (mg/dl) | 259 | ±17 | **509*** | **±112** | 244 | ±24 | 283 | ±36 | 257 | ±31 | 272 | ±13 |
| Phosphate (mg/dl) | 7.3 | ±0.2 | 14.2 | ±4.9 | 6.6 | ±0.6 | 7.0 | ±0.4 | 7.4 | ±0.2 | 7.5 | ±0.1 |
| Bicarbonate (mmol/L) | 25.8 | ±0.5 | 17.4 | ±5.3 | 26.5 | ±0.7 | 27.3 | ±0.3 | 28.0 | ±0.4 | 24.7 | ±0.3 |
| Sodium (mmol/L) | 142.0 | ±0.4 | 139.0 | ±1.9 | 140.3 | ±0.8 | 140.7 | ±0.6 | 141.7 | ±0.8 | 142.3 | ±0.3 |
| Potassium (mmol/L) | 4.6 | ±0.1 | 6.3 | ±0.3 | 4.7 | ±0.3 | 4.7 | ±4.5 | 0.2 | ±12 | 4.6 | ±0.2 |

*$p < 0.05$ with respect to the control group. $N = 3$–6 animals per group.

that preferentially inhibits smooth muscle cell growth offers significant promise over the chemotherapeutics currently approved for prevention of restenosis.

Several studies have demonstrated inhibition of neointimal hyperplasia using NO-based approaches in animal models. These approaches include inhalational NO therapy (12), L-arginine supplementation (38), systemic administration of NO donors (29, 40), gene transfer therapy (47, 57, 59), and local delivery of NO donors (16, 26, 34, 42, 46). However, these therapies have had limited clinical utility and interest due to a variety of concerns, which include the absence of a significant and durable effect, systemic side effects, safety concerns, and, importantly, complicated delivery schemes. We have previously shown inhibition of neointimal hyperplasia using an NO-releasing nanofiber gel that was directly applied to the periadventitial surface of the injured vessel (26).

However, our current study represents the first example that couples the local inhibitory effect of NO-derived species on neointimal hyperplasia with targeted systemic delivery of a nanostructure. We show inhibition of cell proliferation *in vivo* with the targeted SNO nanofiber at 3 days, a time point normally shown to have active cellular proliferation (1, 9, 13). This early inhibition of proliferation correlates with a local increase in nitrotyrosine staining, an indicator of nitrosative stress. The presence and redox effects of our therapy at 3 days are clinically advantageous since we previously reported that a 5-min exposure to NO in the intravascular space is sufficient to inhibit neointimal hyperplasia at 2 weeks (22).

Hence, the early inhibition of cell proliferation observed could indeed account for the inhibition of neointimal hyperplasia observed at 2 weeks, even if the nanofibers persist at the site of injury only for 3 days. Moreover, our study shows a durable effect of the NO-mediated therapy up to 7 months after arterial injury, highlighting the importance of early intervention. Another advantage of this therapy is that it uses a simple peripheral intravenous injection and thus could be easily redosed as necessary, making this therapy even more attractive for clinical use. Thus, this approach offers great versatility in terms of both targeting to a site of interest and providing a platform to deliver a wide range of therapeutic molecules, depending on the clinical need.

Another benefit of the model targeted therapy described here relates to the type of NO functionalization utilized. The kinetics of RSNO decomposition *in vivo* is difficult to predict as the stability depends on local conditions. However, RSNOs can have bioactive effects by releasing NO or by direct reactivity with biological targets. In the case of release of NO, the resulting thiol could potentially be regenerated *in vivo* through reaction with endogenous circulating RSNOs and continue to be a source of NO-like activity at the site of injury as long as the nanofiber remains bound to the artery. Indeed, we showed that our targeted nanofiber remains bound to the injured artery for 3 days and that the SH-PA can accept an NO moiety *via* transnitrosylation with another RSNO. Moreover, we showed an increase in plasma RSNO, suggesting that the SNO nanofibers could transnitrosylate plasma proteins.

The chemical nature of the nanofibers poses some limitations to this work that require further investigation. First, we could not establish if the inhibition of neointimal hyperplasia observed with the targeted SNO nanofiber is due to an effect of NO released from the nanofiber or due to the biological effect of the RSNO. It is possible that the SNO nanofiber transnitrosylates a small molecule that could carry the SNO signal. However, we did not observe evidence of S-nitrosylation at

3 days using an antibody against S-nitrosocysteine or at 2 h with the biotin-switch assay. This could be due to either the time at which we evaluated protein S-nitrosylation or to the nature of our assay as there are some specificity limitations with the anti-S-nitrosocysteine antibody and the S-nitrosylated proteins may have been below the level of detection with these methodologies and the limited amount of tissue we had to assess. On the other hand, if enough NO were to be released, an increase in cGMP would be expected.

However, we did not observe a change in cGMP levels either locally or systemically with our therapy. Thus, we have not identified the biologically active molecule to be NO or an RSNO. Nevertheless, it effectively prevents neointimal development in a durable manner *via* early inhibition of cell proliferation, which correlates with observable changes in the redox balance (increased tyrosine nitration and early increase in plasma RSNO).

Our study on the systemic effects of the targeted SNO nanofiber showed some transient alterations in the hematology variables as well as in the clinical chemistry results. We currently have not determined the etiology of this acute response. However, we have determined that these effects are independent of the presence of the SNO moiety since we observed similar changes with both the SNO and non-SNO nanofibers. Regarding the hematologic variables, we noted a transient shift in the leukocyte differential with an increase in neutrophils and decrease in lymphocytes. This is consistent with the acute injection of a foreign material. Regarding the blood chemistries, there was a small drop in the alanine aminotransferase after injection of the SNO nanofiber that persisted to day 7. This was not observed with the SH nanofiber.

While statistically significant, the change in value was not clinically significant as the values are all within normal limits. We also noted a transient increase in the aspartate aminotransferase, CK, BUN, and glucose 3 h after injection with both the SNO and SH nanofibers that returned to normal at 1 day. This may be due to sequestration of the nanofiber by the liver and/or muscle (with the latter potentially affecting glucose metabolism as well).

Further studies will be required to establish biological safety, including a detailed analysis of the biodistribution, metabolism, and clearance of the targeted nanostructures. Last, while collagen IV is an attractive target for the prevention of arterial restenosis, discovery of a peptide epitope unique to the site of arterial injury may result in even greater specificity and efficacy of a targeted intravascular therapy for use in humans.

In conclusion, we describe the development and evaluation of a nanofiber that delivers an SNO locally to the site of arterial injury *via* a systemic intravenous injection and prevents the development of neointimal hyperplasia. To our knowledge, this is the first report of a systemically delivered therapy designed to release NO locally at the site of arterial injury through direct targeting of the supramolecular nanostructure. This therapy has clinical promise given its simplicity, efficacy, ability to be redosed, and apparent safety. In addition, this work has far-reaching implications for other disease processes that may benefit from targeted delivery of therapeutic agents administered systemically. Future directions will include evaluation of this therapy in a preclinical large animal model as well as in the setting of older age and atherosclerosis.

## Materials and Methods

### *Study approval*

All animal procedures were performed in accordance with the Guide for the Care and Use of Laboratory Animals (National Institutes of Health Publication 85-23, 1996) and approved by the Northwestern University Animal Care and Use Committee. The number of rats randomized to each treatment group ($N = 6–7$) was calculated using a power of 0.8, difference in means of 0.2, standard deviation of 0.1, and $p$-value of 0.05.

### *PA synthesis and functionalization*

The collagen-targeting PAs and peptides were synthesized using standard Fmoc solid-phase synthesis conditions as described previously (52). Briefly, coupling reactions included Fmoc-amino acids (4 equiv), *O*-(Benzotriazol-1-yl)-*N*,*N*,*N*′,*N*′-tetramethyluronium hexafluorophosphate (3.95 equiv), and diisopropylethylamine (6 equiv) in dimethylformamide. For the aliphatic tail of collagen-targeting PA [sequence KLVWLPKCK2A2V2K(C12)], lauric acid was attached to the ε-amine of a lysine, which was deprotected by selective removal of the 4-methyltrityl group using 2% trifluoroacetic acid (TFA) +5% triisopropylsilane (TIPS) in $CH_2Cl_2$. Cleavage was performed using a TFA/TIPS/$H_2O$/2,2′-(Ethylenedioxy) diethanethiol mixture (90:2.5:2.5:5).

Purification by preparative-scale HPLC was carried out on a Varian Prostar 210 HPLC system, eluting with 2% acetonitrile (ACN) to 100% ACN in water on a Phenomenex Jupiter Proteo C12 column (150 × 30 mm). TFA (0.1%) was added to both mobile phases to aid PA solubility during purification. Product-containing fractions were confirmed by ESI-MS (Agilent 6510 Q-TOF LC/MS), combined, and lyophilized after removing ACN by rotary evaporation.

S-nitrosylation of PAs was achieved using slightly modified methods, as previously described (35). Briefly, 1 mmol/L PA was dissolved in acidic solution (pH 3) with 1 equiv of $NaNO_2$ and 50 μmol/L pentetic acid for 1 h and protected from light. The SNO-PA was then dialyzed, lyophilized, and stored at −20°C. For material characterization, *in vitro*, and *in vivo* experiments, SNO-PA powder was resuspended in phosphate-buffered saline (PBS).

### *Material characterization*

cryo-TEM specimens were prepared using an FEI Vitrobot by blotting in 95% humidity and subsequently plunging lacey carbon grids into liquid ethane. Images were taken for cryo-TEM using a JEOL 1230 transmission electron microscope operating at 100 keV equipped with a Gatan camera. Samples were dissolved at 250 μmol/L in PBS and aged for 1–2 h before plunging.

SAXS experiments were performed at the Advanced Photon Source, Argonne National Laboratory. The X-ray energy (15 keV) was selected using a double-crystal monochromator with a 30 mm offset. Samples were dissolved at a concentration of 5 mmol/L in PBS and placed in 1.5-mm quartz capillary tubes. The typical incident X-ray flux on the sample was $\sim 1 \times 1012$ photons/s with a $0.2 \times 0.3\,mm^2$ collimator, and samples were exposed for 4 s.

The one-dimensional scattering profiles were obtained by azimuthal integration of the two-dimensional patterns, with

scattering from the capillaries and PBS buffer subtracted as background. Scattering profiles were then plotted on a relative scale as a function of the scattering vector $q=(4\pi/\lambda)\sin(\theta/2)$, where $\theta$ is the scattering angle. Fits were performed using a polydisperse core-shell cylinder model for the nanofibers. The polydisperse core-shell cylinder fit has been described previously (36). Polydispersity was introduced using a log-normal distribution for the core radius.

### NO measurements and release

Lyophilized SNO-PA powder was resuspended in $H_2O$. Absorption measurements of the SNO group formation were done using a 96-well M5 plate reader, in triplicate. SNO decomposition was assessed by monitoring the SNO group spectrophotometrically at 350 nm. NO release was assayed using the Apollo free radical analyzer equipped with an ISO-NOPF100 NO electrode (World Precision Instruments). An aliquot of the nanofiber or the SNO nanofiber (5 $\mu$mol/L) was added to a vial containing 10 mL of PBS with or without ascorbate (50 $\mu$mol/L) and copper (1–5 $\mu$mol/L). NO release was also assayed using the Sievers NO Analyzer (GE Instruments). SNO nanofiber (1.5 nmoles) was injected into the analyzer containing ascorbate (1 mmol/L) and copper (10 $\mu$mol/L).

### Transnitrosylation reaction

To assess the reaction of RSNOs with reduced thiols, the SNO-PA nanofiber was incubated with GSH and the SH-PA nanofiber was incubated with GSNO at 200 $\mu$mol/L, 37°C, and pH 7.4 over time. Every 90 min an aliquot was analyzed by HPLC with electrochemical detection to quantify GSH, GSNO, SH-PA, and SNO-PA. The separation method was a standard gradient eluting with 2% ACN to 100% ACN in water over 30 min on a Phenomenex Kinetex column (5 $\mu$m XB-C18, 100 Å, 150×4.6 mm). TFA (0.1%) was added to both mobile phases. The detection potentials were set at 400, 600, and 900 mV.

### Biochemical analyses

Carotid arteries were harvested 2 h after surgery and immediately frozen in liquid nitrogen. Lysates were obtained by homogenization with a glass tapered tissue grinder in HEPES with 0.1% Triton X-100 and protease inhibitors. cGMP was assayed in carotid lysates and plasma using an acetylated direct cGMP kit (AbCam) according to the manufacturer's specifications. Protein S-nitrosylation was assessed *via* a biotin-switch assay as previously described (15). Reactive nitrogen species (NOx) in plasma, nitrite, and D-nitrosothiols in plasma were determined using the triiodide method, as previously described (33). The assays were performed using ozone-based chemiluminescence detection with a Sievers Nitric Oxide Analyzer (GE Analytical Instruments).

### Cell proliferation and viability assays

VSMC proliferation was assayed using the $^3$H-thymidine incorporation assays previously described (53, 54). For the viability assay, VSMCs were seeded onto 12-well plates at a density of 30,000 cells/well. Cells were allowed to adhere overnight, followed by serum starvation for 24 h to induce cell synchronization. Cells were then exposed to the different treatment groups. After 24 h, viability and cell death were assessed using the Muse benchtop cytometer (EMD Millipore) according to the manufacturer's specifications.

### Animal surgery

Adult male Sprague-Dawley rats, weighing 350–400 g, underwent carotid artery balloon injury as previously described (58). After balloon injury, the arteriotomy was ligated and heparin (50 U/kg) was injected through the tail vein of the animal. After the heparin circulated for 10 min, 5 or 2.5 mg of the different nanostructures, dissolved in Hanks Balanced Salt Solution, was injected *via* the tail vein into the animal. Blood flow was then restored to the common carotid artery and the neck incision was closed. Rats were euthanized at 1 h, 1, 2, 4, 6, 14 days, or 7 months postinjection based on the experiment being conducted. $N=6$ per treatment group except for the 7-month time point in which $N=7$ per treatment group.

Blood pressure was monitored in rats that were awake before surgery, 3 h after surgery, and 1 day after surgery using the noninvasive Volume Pressure Recording CODA System (Kent Scientific). Some animals received an intravenous injection of Evans Blue dye (0.5 mL of 0.5%; Sigma) immediately before sacrifice to identify denuded endothelial surfaces. Following *in situ* perfusion with PBS, carotid arteries were removed and photographed. Areas of denuded endothelium were identified by blue staining, and the portion of the injured area stained blue was quantitated using ImageJ (NIH). Some animals received BrdU (100 mg/kg) 24 h and 1 h before sacrifice to label rapidly proliferating cells. *In vivo* cell proliferation was assessed by BrdU immunohistochemistry as previously described (55).

### Tissue processing

Carotid arteries were harvested after *in situ* perfusion with PBS (250 ml) and placed in 2% paraformaldehyde overnight for fixation. Tissue was processed as previously described (58).

### Morphometric analysis

Carotid arteries harvested 14 days and 7 months after injury were examined histologically for evidence of neointimal hyperplasia using routine hematoxylin and eosin staining. Digital images were collected with light microscopy using an Olympus BHT microscope with a 10× objective. Six to ten evenly spaced sections through each injured carotid artery were morphometrically analyzed. Lumen area, intima area (I), media area (M), and I/M area ratio (arbitrary units) were obtained using ImageJ software (National Institutes of Health). Percent occlusion was calculated as follows: (Lumen area/(Lumen + Intima area)) ×100.

### Binding duration and quantification study

SNO PA was coassembled with PA fluorescently tagged with Alexa-Fluor 546 in a 98:2 ratio as described previously (39). To determine the duration of binding of the nanofiber to the site of injury, fluorescent nanofibers (2.5 mg) were injected immediately after balloon injury as described in the

animal surgery section and carotid arteries were harvested at different time points. After tissue processing, digital images were acquired using a Zeiss LSM-510 microscope with a 20× objective. Four high-magnification pictures were acquired per slide, providing 12–24 technical replicates per animal to analyze. Quantification was performed using ImageJ (National Institutes of Health) after images were thresholded and converted to binary, and the total area of positive staining was quantified.

To quantify the total amount of nanofiber that binds to the carotid artery after systemic injection, carotid arteries were harvested 1 h after surgery and immediately frozen in liquid nitrogen. Lysates were obtained by homogenization with a glass tapered tissue grinder in HEPES with 0.1% Triton X-100 and protease inhibitors. The fluorescence recovered was read in a Biotek Cytation 3 plate reader (Biotek) using 550 nm/580 nm as excitation and emission wavelengths, respectively. The background fluorescence recovered from contralateral uninjured carotid artery lysates was used as a paired blank. Carotid arteries from untreated animals were spiked with a known amount (50 pg) of fluorescent SNO nanofiber and used as a positive control and quantification reference.

### *Immunofluorescence staining*

From each animal, 3–6 evenly spaced carotid artery sections from the area of injury were stained with anti-ED1 antibody for evidence of macrophage infiltration. Frozen sections were fixed in 2% paraformaldehyde. Sections were incubated with the primary antibody (anti-ED1, Cat#sc59103; Santa Cruz Biotechnology) at a 1:50 dilution in IHC-TEK antibody diluent (IHC World) for 1 h at room temperature, followed by secondary 1:500 in PBS for 1 h. For evaluation of nitrotyrosine and S-nitrosocysteine, carotid artery cross sections were incubated with an antinitrotyrosine antibody (Cat# ab61392; Abcam) at a 1:1000 dilution or an anti-S-nitrosocysteine antibody (Cat# ab94930; Abcam) at a 1:500 dilution in IHC-Tek antibody diluent (IHC World) for 1 h at room temperature.

After a 2-min rinse of PBS, the sections were incubated with an F(ab′)2-goat anti-mouse IgG (H + L) secondary antibody (Alexa Fluor® 555 conjugate, Cat#A-2145; Thermo Fisher Scientific) at 1:500 for the antinitrotyrosine primary, and 1:1000 for the anti-S-nitrosocysteine primary, in PBS for 1 h at room temperature. Nuclei were stained with 4′,6-diamidino-2-phenylindole 1:500 in PBS for 1 min (Cat#D3571; Thermo Fisher Scientific). Finally, slides were coverslipped with ProLong Gold (Cat#P36930; Thermo Fisher Scientific). Digital images were acquired using a Zeiss LSM-510 microscope with a 20×objective, HE Cy3 filter (Zeiss filter #43), using excitation and emission wavelengths of 550–575 nm and 605–670 nm, respectively. Images were analyzed in the same manner described in the binding duration study above.

### *Blood chemistry*

Blood was collected at different time points after tail vein injection of 5 mg of the targeted nanofiber or the targeted SNO nanofiber. Hematology, clinical chemistries, and coagulation panels were performed off-site by IDEXX Laboratories, Inc. Functional complement assay was performed according to published methods (2). Briefly, commercial sheep red blood cells (Innovative Research, Inc.) were washed, and then sensitized with 1.4 mg/ml hemolysin (Sigma). Human serum (Sigma) was exposed to the targeted SNO nanofibers (0.5 and 1 mg/ml) at 37°C for 1 h. Sensitized sheep red blood cells were incubated with the treated human serum at 37°C for 1 h, and cell lysis was assessed at 412 nm.

### *Statistical analyses*

All results are presented as mean ± the standard error of the mean. Differences between multiple groups for nonpaired parametric data were analyzed using one-way analysis of variance with the Student–Newman–Keuls *post hoc* test for all pairwise comparisons. Differences for paired data were analyzed using repeated-measures analysis of variance (ANOVA). Non-normally distributed data were analyzed using a Kruskal–Wallis ANOVA on ranks with the Student–Newman–Keuls *post hoc* test for pairwise comparisons. Differences between two groups were analyzed using a two-tailed *t*-test. All statistical analyses were performed using either SigmaPlot v10.0 (Systat Software, Inc.) or SAS (SAS Institute, Inc.). Statistical significance was assumed when $p < 0.05$.

## Acknowledgments

The authors acknowledge the Peptide Synthesis Core Facility of the Simpson Querrey Institute for BioNanotechnology at Northwestern University. SAXS results were obtained at the DuPont-Northwestern-Dow Collaborative Access Team (DND-CAT) located at Sector 5 of the Advanced Photon Source (APS). DND-CAT is supported by E.I. DuPont de Nemours and Co., The Dow Chemical Company, and Northwestern University. Use of the APS, an Office of Science User Facility operated for the U.S. Department of Energy (DOE) Office of Science by Argonne National Laboratory, was supported by the U.S. DOE under Contract No. DE-AC02-06CH11357.

This research was supported by the NIH (Bioengineering Research Partnership 1R01HL116577-01), a Catalyst Award from the Louis A. Simpson and Kimberly K. Querrey Center for Regenerative Nanomedicine at Northwestern University, and research seed funding from the Feinberg School of Medicine, Northwestern University. H.A.K. was supported by an NIH T32 vascular surgery training grant (T32HL094293); E.S.M.B. is supported by a postdoctoral research fellowship from the American Heart Association (13POST16090011); and T.J.M. was supported by a graduate research fellowship from the National Science Foundation. The authors acknowledge Dr. Nick Tsihlis for his critical review of the manuscript and Mrs. Lynnette Dangerfield for her administrative and editorial assistance.

## Author Disclosure Statement

No competing financial interests exist.

## References

1. Angelini A, Visona A, Calabrese F, Pettenazzo E, Yacoub A, Valente M, Bonandini EM, Jori G, Pagnan A, and Thiene G. Time course of apoptosis and prolideration in vascular

smooth muscle cells after balloon angioplasty. *Basic Appl Myol* 12: 33–42, 2012.
2. ASTM. *Practice for Testing for Whole Complement Activation in Serum by Solid Materials*. West Conshohocken, PA: ASTM International, 2013.
3. Bahnson ES, Koo N, Cantu-Medellin N, Tsui AY, Havelka GE, Vercammen JM, Jiang Q, Kelley EE, and Kibbe MR. Nitric oxide inhibits neointimal hyperplasia following vascular injury via differential, cell-specific modulation of SOD-1 in the arterial wall. *Nitric Oxide* 44: 8–17, 2015.
4. Chan JM, Rhee JW, Drum CL, Bronson RT, Golomb G, Langer R, and Farokhzad OC. *In vivo* prevention of arterial restenosis with paclitaxel-encapsulated targeted lipid-polymeric nanoparticles. *Proc Natl Acad Sci U S A* 108: 19347–19352, 2011.
5. Chan JM, Zhang L, Tong R, Ghosh D, Gao W, Liao G, Yuet KP, Gray D, Rhee JW, Cheng J, Golomb G, Libby P, Langer R, and Farokhzad OC. Spatiotemporal controlled delivery of nanoparticles to injured vasculature. *Proc Natl Acad Sci U S A* 107: 2213–2218, 2010.
6. Choi CH, Alabi CA, Webster P, and Davis ME. Mechanism of active targeting in solid tumors with transferrin-containing gold nanoparticles. *Proc Natl Acad Sci U S A* 107: 1235–1240, 2010.
7. Clowes AW and Clowes MM. Kinetics of cellular proliferation after arterial injury. II. Inhibition of smooth muscle growth by heparin. *Lab Invest* 52: 611–616, 1985.
8. Clowes AW, Clowes MM, and Reidy MA. Kinetics of cellular proliferation after arterial injury. III. Endothelial and smooth muscle growth in chronically denuded vessels. *Lab Invest* 54: 295–303, 1986.
9. Clowes AW, Reidy MA, and Clowes MM. Kinetics of cellular proliferation after arterial injury. I. Smooth muscle growth in the absence of endothelium. *Lab Invest* 49: 327–333, 1983.
10. Cui H, Webber MJ, and Stupp SI. Self-assembly of peptide amphiphiles: from molecules to nanostructures to biomaterials. *Biopolymers* 94: 1–18, 2010.
11. Davies MG, Kim JH, Dalen H, Makhoul RG, Svendsen E, and Hagen PO. Reduction of experimental vein graft intimal hyperplasia and preservation of nitric oxide-mediated relaxation by the nitric oxide precursor L-arginine. *Surgery* 116: 557–568, 1994.
12. Davis ME, Zuckerman JE, Choi CH, Seligson D, Tolcher A, Alabi CA, Yen Y, Heidel JD, and Ribas A. Evidence of RNAi in humans from systemically administered siRNA via targeted nanoparticles. *Nature* 464: 1067–1070, 2010.
13. Durand E, Mallat Z, Addad F, Vilde F, Desnos M, Guerot C, Tedgui A, and Lafont A. Time courses of apoptosis and cell proliferation and their relationship to arterial remodeling and restenosis after angioplasty in an atherosclerotic rabbit model. *J Am Coll Cardiol* 39: 1680–1685, 2002.
14. Farokhzad OC, Jon S, Khademhosseini A, Tran TN, Lavan DA, and Langer R. Nanoparticle-aptamer bioconjugates: a new approach for targeting prostate cancer cells. *Cancer Res* 64: 7668–7672, 2004.
15. Forrester MT, Foster MW, Benhar M, and Stamler JS. Detection of protein S-nitrosylation with the biotin-switch technique. *Free Radic Biol Med* 46: 119–126, 2009.
16. Fulton GJ, Davies MG, Barber L, Gray JL, Svendsen E, and Hagen PO. Local effects of nitric oxide supplementation and suppression in the development of intimal hyperplasia in experimental vein grafts. *Eur J Vasc Endovasc Surg* 15: 279–289, 1998.
17. Furchgott RF and Zawadzki JV. The obligatory role of endothelial cells in the relaxation of arterial smooth muscle by acetylcholine. *Nature* 288: 373–376, 1980.
18. Garg UC and Hassid A. Nitric oxide-generating vasodilators and 8-bromo-cyclic guanosine monophosphate inhibit mitogenesis and proliferation of cultured rat vascular smooth muscle cells. *J Clin Invest* 83: 1774–1777, 1989.
19. Guo JP, Panday MM, Consigny PM, and Lefer AM. Mechanisms of vascular preservation by a novel NO donor following rat carotid artery intimal injury. *Am J Physiol* 269: H1122–H1131, 1995.
20. Haldar SM and Stamler JS. S-nitrosylation: integrator of cardiovascular performance and oxygen delivery. *J Clin Invest* 123: 101–110, 2013.
21. Hartgerink JD, Beniash E, and Stupp SI. Self-assembly and mineralization of peptide-amphiphile nanofibers. *Science* 294: 1684–1688, 2001.
22. Havelka GE, Moreira ES, Rodriguez MP, Tsihlis ND, Wang Z, Martinez J, Hrabie JA, Kiefer LK, and Kibbe MR. Nitric oxide delivery via a permeable balloon catheter inhibits neointimal growth after arterial injury. *J Surg Res* 180: 35–42, 2013.
23. Hess DT and Stamler JS. Regulation by S-nitrosylation of protein post-translational modification. *J Biol Chem* 287: 4411–4418, 2012.
24. Hrabie JA and Keefer LK. Chemistry of the nitric oxide-releasing diazeniumdiolate (''nitrosohydroxylamine'') functional group and its oxygen-substituted derivatives. *Chem Rev* 102: 1135–1154, 2002.
25. Hrkach J, Von Hoff D, Mukkaram Ali M, Andrianova E, Auer J, Campbell T, De Witt D, Figa M, Figueiredo M, Horhota A, Low S, McDonnell K, Peeke E, Retnarajan B, Sabnis A, Schnipper E, Song JJ, Song YH, Summa J, Tompsett D, Troiano G, Van Geen Hoven T, Wright J, LoRusso P, Kantoff PW, Bander NH, Sweeney C, Farokhzad OC, Langer R, and Zale S. Preclinical development and clinical translation of a PSMA-targeted docetaxel nanoparticle with a differentiated pharmacological profile. *Sci Transl Med* 4: 128ra39, 2012.
26. Kapadia MR, Chow LW, Tsihlis ND, Ahanchi SS, Eng JW, Murar J, Martinez J, Popowich DA, Jiang Q, Hrabie JA, Saavedra JE, Keefer LK, Hulvat JF, Stupp SI, and Kibbe MR. Nitric oxide and nanotechnology: a novel approach to inhibit neointimal hyperplasia. *J Vasc Surg* 47: 173–182, 2008.
27. Keefer LK. Progress toward clinical application of the nitric oxide-releasing diazeniumdiolates. *Annu Rev Pharmacol Toxicol* 43: 585–607, 2003.
28. Kubes P, Suzuki M, and Granger DN. Nitric oxide: an endogenous modulator of leukocyte adhesion. *Proc Natl Acad Sci U S A* 88: 4651–4655, 1991.
29. Lablanche JM, Grollier G, Lusson JR, Bassand JP, Drobinski G, Bertrand B, Battaglia S, Desveaux B, Juilliere Y, Juliard JM, Metzger JP, Coste P, Quiret JC, Dubois-Rande JL, Crochet PD, Letac B, Boschat J, Virot P, Finet G, Le Breton H, Livarek B, Leclercq F, Beard T, Giraud T, and Bertrand ME. Effect of the direct nitric oxide donors linsidomine and molsidomine on angiographic restenosis after coronary balloon angioplasty. The ACCORD Study. Angioplastic Coronaire Corvasal Diltiazem. *Circulation* 95: 83–89, 1997.

30. Lee JS, Adrie C, Jacob HJ, Roberts JD, Jr, Zapol WM, and Bloch KD. Chronic inhalation of nitric oxide inhibits neointimal formation after balloon-induced arterial injury. *Circ Res* 78: 337–342, 1996.
31. Lichtenstein O, Safar ME, Poitevin P, and Levy BI. Biaxial mechanical properties of carotid arteries from normotensive and hypertensive rats. *Hypertension* 26: 15–19, 1995.
32. Lima B, Forrester MT, Hess DT, and Stamler JS. S-nitrosylation in cardiovascular signaling. *Circ Res* 106: 633–646, 2010.
33. MacArthur PH, Shiva S, and Gladwin MT. Measurement of circulating nitrite and S-nitrosothiols by reductive chemiluminescence. *J Chromatogr B Analyt Technol Biomed Life Sci* 851: 93–105, 2007.
34. Marks DS, Vita JA, Folts JD, Keaney JF, Jr, Welch GN, and Loscalzo J. Inhibition of neointimal proliferation in rabbits after vascular injury by a single treatment with a protein adduct of nitric oxide. *J Clin Invest* 96: 2630–2638, 1995.
35. Mathews WR and Kerr SW. Biological activity of S-nitrosothiols: the role of nitric oxide. *J Pharmacol Exp Ther* 267: 1529–1537, 1993.
36. Matson JB and Stupp SI. Self-assembling peptide scaffolds for regenerative medicine. *Chem Commun (Camb)* 48: 26–33, 2012.
37. Matsuzawa T, Nomura M, and Unno T. Clinical pathology reference ranges of laboratory animals. Working Group II, Nonclinical Safety Evaluation Subcommittee of the Japan Pharmaceutical Manufacturers Association. *J Vet Med Sci* 55: 351–362, 1993.
38. McNamara DB, Bedi B, Aurora H, Tena L, Ignarro LJ, Kadowitz PJ, and Akers DL. L-arginine inhibits balloon catheter-induced intimal hyperplasia. *Biochem Biophys Res Commun* 193: 291–296, 1993.
39. Moyer TJ, Kassam HA, Bahnson ES, Morgan CE, Tantakitti F, Chew TL, Kibbe MR, and Stupp SI. Shape-dependent targeting of injured blood vessels by peptide amphiphile supramolecular nanostructures. *Small* 11:2750–2755, 2015.
40. Napoli C, Cirino G, Del Soldato P, Sorrentino R, Sica V, Condorelli M, Pinto A, and Ignarro LJ. Effects of nitric oxide-releasing aspirin versus aspirin on restenosis in hypercholesterolemic mice. *Proc Natl Acad Sci U S A* 98: 2860–2864, 2001.
41. Palmerini T, Biondi-Zoccai G, Della Riva D, Stettler C, Sangiorgi D, D'Ascenzo F, Kimura T, Briguori C, Sabate M, Kim HS, De Waha A, Kedhi E, Smits PC, Kaiser C, Sardella G, Marullo A, Kirtane AJ, Leon MB, and Stone GW. Stent thrombosis with drug-eluting and bare-metal stents: evidence from a comprehensive network meta-analysis. *Lancet* 379: 1393–1402, 2012.
42. Pearce CG, Najjar SF, Kapadia MR, Murar J, Eng J, Lyle B, Aalami OO, Jiang Q, Hrabie JA, Saavedra JE, Keefer LK, and Kibbe MR. Beneficial effect of a short-acting NO donor for the prevention of neointimal hyperplasia. *Free Radic Biol Med* 44: 73–81, 2008.
43. Popowich DA, Vavra AK, Walsh CP, Bhikhapurwala HA, Rossi NB, Jiang Q, Aalami OO, and Kibbe MR. Regulation of reactive oxygen species by p53: implications for nitric oxide-mediated apoptosis. *Am J Physiol Heart Circ Physiol* 298: H2192–H2200, 2010.
44. Qian X, Peng XH, Ansari DO, Yin-Goen Q, Chen GZ, Shin DM, Yang L, Young AN, Wang MD, and Nie S. *In vivo* tumor targeting and spectroscopic detection with surface-enhanced Raman nanoparticle tags. *Nat Biotechnol* 26: 83–90, 2008.
45. Radomski MW, Palmer RM, and Moncada S. Endogenous nitric oxide inhibits human platelet adhesion to vascular endothelium. *Lancet* 2: 1057–1058, 1987.
46. Schwarzacher SP, Lim TT, Wang BY, Kernoff RS, Niebauer J, Cooke JP, and Yeung AC. Local intramural delivery of L-arginine enhances nitric oxide generation and inhibits lesion formation after balloon angioplasty. *Circulation* 95: 1863–1869, 1997.
47. Shears LL, Kibbe MR, Murdock AD, Billiar TR, Lizonova A, Kovesdi I, Watkins SC, and Tzeng E. Efficient inhibition of intimal hyperplasia by adenovirus-mediated inducible nitric oxide synthase gene transfer to rats and pigs *in vivo*. *J Am Coll Surg* 187: 295–306, 1998.
48. Silva GA, Czeisler C, Niece KL, Beniash E, Harrington DA, Kessler JA, and Stupp SI. Selective differentiation of neural progenitor cells by high-epitope density nanofibers. *Science* 303: 1352–1355, 2004.
49. Soukasene S, Toft DJ, Moyer TJ, Lu H, Lee HK, Standley SM, Cryns VL, and Stupp SI. Antitumor activity of peptide amphiphile nanofiber-encapsulated camptothecin. *ACS Nano* 5: 9113–9121, 2011.
50. Stamler JS. S-nitrosothiols and the bioregulatory actions of nitrogen oxides through reactions with thiol groups. *Curr Top Microbiol Immunol* 196: 19–36, 1995.
51. Stettler C, Wandel S, Allemann S, Kastrati A, Morice MC, Schomig A, Pfisterer ME, Stone GW, Leon MB, de Lezo JS, Goy JJ, Park SJ, Sabate M, Suttorp MJ, Kelbaek H, Spaulding C, Menichelli M, Vermeersch P, Dirksen MT, Cervinka P, Petronio AS, Nordmann AJ, Diem P, Meier B, Zwahlen M, Reichenbach S, Trelle S, Windecker S, and Juni P. Outcomes associated with drug-eluting and bare-metal stents: a collaborative network meta-analysis. *Lancet* 370: 937–948, 2007.
52. Toft DJ, Moyer TJ, Standley SM, Ruff Y, Ugolkov A, Stupp SI, and Cryns VL. Coassembled cytotoxic and pegylated peptide amphiphiles form filamentous nanostructures with potent antitumor activity in models of breast cancer. *ACS Nano* 6: 7956–7965, 2012.
53. Tsihlis ND, Murar J, Kapadia MR, Ahanchi SS, Oustwani CS, Saavedra JE, Keefer LK, and Kibbe MR. Isopropylamine NONOate (IPA/NO) moderates neointimal hyperplasia following vascular injury. *J Vasc Surg* 51: 1248–1259, 2010.
54. Tsihlis ND, Oustwani CS, Vavra AK, Jiang Q, Keefer LK, and Kibbe MR. Nitric oxide inhibits vascular smooth muscle cell proliferation and neointimal hyperplasia by increasing the ubiquitination and degradation of UbcH10. *Cell Biochem Biophys* 60: 89–97, 2011.
55. Tsihlis ND, Vavra AK, Martinez J, Lee VR, and Kibbe MR. Nitric oxide is less effective at inhibiting neointimal hyperplasia in spontaneously hypertensive rats. *Nitric Oxide* 35: 165–174, 2013.
56. Vance D, Martin J, Patke S, and Kane RS. The design of polyvalent scaffolds for targeted delivery. *Adv Drug Deliv Rev* 61: 931–939, 2009.
57. Varenne O, Pislaru S, Gillijns H, Van Pelt N, Gerard RD, Zoldhelyi P, Van de Werf F, Collen D, and Janssens SP. Local adenovirus-mediated transfer of human endothelial nitric oxide synthase reduces luminal narrowing after coronary angioplasty in pigs. *Circulation* 98: 919–926, 1998.
58. Vavra AK, Havelka GE, Martinez J, Lee VR, Fu B, Jiang Q, Keefer LK, and Kibbe MR. Insights into the effect of

nitric oxide and its metabolites nitrite and nitrate at inhibiting neointimal hyperplasia. *Nitric Oxide* 25: 22–30, 2011.
59. von der L, Gibbons GH, Morishita R, Lewis NP, Zhang L, Nakajima M, Kaneda Y, Cooke JP, and Dzau VJ. Gene therapy inhibiting neointimal vascular lesion: *in vivo* transfer of endothelial cell nitric oxide synthase gene. *Proc Natl Acad Sci U S A* 92: 1137–1141, 1995.
60. Ziche M, Morbidelli L, Masini E, Amerini S, Granger HJ, Maggi CA, Geppetti P, and Ledda F. Nitric oxide mediates angiogenesis *in vivo* and endothelial cell growth and migration *in vitro* promoted by substance P. *J Clin Invest* 94: 2036–2044, 1994.

Address correspondence to:
*Dr. Melina R. Kibbe*
*Simpson Querrey Institute for BioNanotechnology*
*Northwestern University*
*303 E. Superior, Suite 11-107*
*Chicago, IL 60611-2875*

*E-mail:* mkibbe@northwestern.edu

Date of first submission to ARS Central, April 17, 2015; date of final revised submission, October 20, 2015; date of acceptance, November 20, 2015.

**Abbreviations Used**

ACN = acetonitrile
ANOVA = analysis of variance
BUN = blood urea nitrogen
cGMP = cyclic guanosine monophosphate
CK = creatine kinase
Cryo-TEM = cryogenic transmission electron microscopy
Cu = copper
ESI-MS = electrospray ionization mass spectrometry
GSH = glutathione
GSNO = S-nitrosoglutathione
HPLC = high-performance liquid chromatography
I/M = intima to media
MAP = mean arterial pressure
NO = nitric oxide
PA = peptide amphiphile
PBS = phosphate-buffered saline
RSNO = S-nitrosothiol
SAXS = small-angle X-ray scattering
SEM = standard error of the mean
SNO = S-nitrosyl
TFA = trifluoroacetic acid
TIPS = triisopropylsilane
VSMC = vascular smooth muscle cell
WBC = white blood cell